Trabecular architecture and joint loading of the proximal humerus in extant hominoids,

Ateles*, and *Australopithecus africanus

Tracy L. Kivell[1,2,3*], Rebecca Davenport[4], Jean-Jacques Hublin[2], J. Francis Thackeray[3], Matthew M. Skinner[1,2,3]

[1] School of Anthropology and Conservation, University of Kent, Canterbury, United Kingdom

[2] Department of Human Evolution, Max Planck Institute for Evolutionary Anthropology, Leipzig Germany

[3] Evolutionary Studies Institute and Center for Excellence in PalaeoSciences, University of the Witwatersrand, South Africa

[4] Department of Anthropology, University College London, United Kingdom

*Corresponding author:
Tracy L. Kivell
School of Anthropology and Conservation
Marlowe Building
University of Kent,
Canterbury CT2 7NR
United Kingdom
t.l.kivell@kent.ac.uk
+44 (0) 1227 82 495

Number of pages of text (including bibliography): 34

Number of figures: 8

Number of tables: 5

Abbreviated title: Trabecular bone of the proximal humerus

Keywords: locomotion, upper limb, hominin, arboreal, cancellous bone

Grant sponsorship: Max Planck Society (TLK, JJH, MMS) and European Research Council Starting Grant #336301 (TLK and MMS)

ABSTRACT

Objectives Several studies have investigated potential functional signals in the trabecular structure of the primate proximal humerus but with varied success. Here we apply for the first time a "whole-epiphyses" approach to analysing trabecular bone in the humeral head with the aim of providing a more holistic interpretation of trabecular variation in relation to habitual locomotor or manipulative behaviors in several extant primates and *Australopithecus africanus*.

Materials and Methods We use a "whole-epiphysis" methodology in comparison to the traditional volume of interest (VOI) approach to investigate variation in trabecular structure and joint loading in the proximal humerus of extant hominoids, *Ateles* and *A. africanus* (StW 328).

Results There are important differences in the quantification of trabecular parameters using a "whole-epiphysis" versus a VOI-based approach. Variation in trabecular structure across knuckle-walking African apes, suspensory taxa, and modern humans was generally consistent with predictions of load magnitude and inferred joint posture during habitual behaviors. Higher relative trabecular bone volume and more isotropic trabeculae in StW 328 suggest *A. africanus* may have still used its forelimbs for arboreal locomotion.

Discussion A whole-epiphysis approach to analysing trabecular structure of the proximal humerus can help distinguish functional signals of joint loading across extant primates and can provide novel insight into habitual behaviors of fossil hominins.

INTRODUCTION

Reconstructing locomotor and manipulative behavior in the primate fossil record is central to discussions surrounding the ways in which extinct taxa interacted with their environments. However, there is often much ambiguity and debate over the functional interpretation of the external morphology of fossils; researchers face the problem of distinguishing between potentially non-functional vestigial reflections of phylogenetic history, and functionally significant markers of actual behaviors. This problem can result in dramatically different reconstructions of behavior in fossil taxa (e.g., Ward, 2002, and references therein).

Contributions to this debate can come from a better understanding of aspects of bony morphology that are more sensitive to loading during life than external bone shape and size. Internal bone structures, including cortical and trabecular bone, may provide this functional insight because they are responsive to the magnitude and direction of mechanical stress during an individual's lifetime, a concept known as bone functional adaptation (Cowin et al., 1985; Currey, 2002; Ruff et al., 2006). Trabecular bone may be particularly useful for reconstructing joint loading and behavior because it remodels faster than cortical bone (Eriksen, 2010). The ways in which trabecular bone's response to mechanical stress may be constrained by, for example, genetic (e.g., Havill et al., 2010) or systemic (e.g., Lieberman, 1996; Chirchir et al., 2015; Tsegai et al., 2018) factors are not fully understood [e.g., Bertram and Swartz, 1991; see Kivell, 2016 for a review]. Furthermore, empirical studies on non-primate animals have found that trabecular bone does not respond to load as predicted in mice (Carlson et al., 2008), and that bony response can vary based on the duration of load (e.g., Skerry and Lanyon, 1995; Lambers et al. 2013) and anatomical region (Räth et al. 2015). However, several empirical studies have demonstrated that altering the direction, magnitude and/or frequency of load is associated with predicted changes in the trabecular structure (e.g., Lanyon, 1974; Bieweiner et al., 1996; Pontzer et al., 2006; van der Meulen et al., 2006; Barak et al., 2011; Wallace et al., 2017). The dynamic response of trabecular bone to loading is also supported by computational analyses, such as finite element modelling, that have demonstrated the strong relationship between variation in trabecular structure and its mechanical

properties (e.g., Odgaard et al., 1997; Kabel et al., 1999; Huiskes et al. 2000; Fox and Keaveny, 2001). As such, analyses of internal bone structure may offer a more direct window into the loads experienced by a particular bone or joint and, ultimately, an individual's behavior, than analyses of external morphology alone.

Locomotor signals in primate trabecular bone of the proximal humerus

Studies that have sought to identify locomotor signals in long bone trabeculae and, in particular, the proximal humerus in extant non-human primates have had varied success. Fajardo and Müller (2001) reported a distinction in trabecular alignment (i.e., degree of anisotropy; DA) in the proximal humerus (and femur) between quadrupedal and suspensory taxa, but found bone volume fraction (bone volume/total volume; BV/TV) to be similar across taxa regardless of locomotor behavior. Ryan and Walker (2010) found that humeral head trabecular structure was consistently different from that of the femoral head across five anthropoid primates, but found no systematic variation in individual trabecular variables within the humeral head across taxa or locomotor groups.

More recent studies using multivariate analyses to investigate several trabecular parameters at once have reported more promising results regarding the relationship between variation in humeral head trabecular structure and different loading regimes. Ryan and Shaw (2012) found that variable suites of trabecular bone features in the humeral head differentiated locomotor groups across eight anthropoid species (although differentiation was clearer in the femoral head). Similarly, Scherf et al. (2013) found significant differences in humeral trabecular structure across three hominoid taxa. Finally, Scherf et al. (2016) found that suites of trabecular bone variables distinguished greater manual activity levels in Neolithic humans relative to recent humans. However, results for individual trabecular variables in these studies did not consistently meet predictions based on variation in humeral loading.

Here we build on this previous work by applying for the first time a "whole-epiphysis" approach to the analysis of humeral head trabecular structure in extant hominoids and spider

monkeys (*Ateles* sp.) in comparison with the traditional volume-of-interest (VOI)-based approach. We aim to provide a more holistic interpretation of trabecular variation in relation to habitual locomotor or manipulative behaviors and, within this comparative context, provide further insight into the upper limb use of *Australopithecus africanus*.

Biomechanical implications of humeral loading regimes

An understanding of the biomechanics of habitual locomotor and/or manipulative behaviors of the study sample is necessary to hypothesise potential relationships between trabecular architecture and humeral loading. *Pan* and *Gorilla* most frequently engage in terrestrial knuckle-walking (Tuttle and Watts, 1985; Hunt, 1991a; Doran, 1997). This locomotor mode involves stereotypical protraction and retraction of the humerus, and thus uniformly repetitive loading of the humeral head in the parasagittal plane (Hunt, 1991b, 1992; Inouye, 1994). Knuckle-walking also generates high compressive joint reaction forces in the humerus due to the combined effect of muscle contraction and gravitational forces acting on the body mass (Carlson and Patel, 2006). *Pan* typically spends more time in the trees than *Gorilla* but in both species the most frequent arboreal locomotor mode is vertical climbing (Tuttle and Watts, 1985; Hunt, 1991a; but see Crompton et al. 2010), which is thought to incur a high degree of gleno-humeral joint strain and is kinematically similar to quadrupedal walking (Hunt, 1991b, 1992; Hanna et al. 2008; Hanna and Schmitt, 2011; Larson and Stern, 2013; Scherf et al., 2013). When arboreal, both *Pan* and, less so *Gorilla*, also infrequently engage in suspensory locomotion, which requires a fully abducted humerus (Tuttle and Watts, 1985; Hunt, 1991a, b; Remis, 1995; Doran, 1997).

Pongo, *Symphalangus* and *Ateles* most frequently engage in arboreal locomotion. The characteristic locomotor mode of *Pongo* is variably classified as orthograde clambering (Cant, 1987, Hunt et al., 1996), quadrumanous clambering (Sugardjito and van Hooff, 1986) and torso-orthograde suspension (Thorpe and Crompton, 2006), all of which broadly describe a slow, upright-torso, irregular climbing pattern in which all four limbs are used in various combinations to grasp substrates in different ways (Sugardjito and van Hooff, 1986; Cant, 1987; Hunt et al., 1996). A

similar locomotor mode is employed frequently during feeding by *Symphalangus* (Fleagle, 1976) and, less often, by *Ateles* (Mittermeier and Fleagle, 1976). Both *Symphalangus* and *Ateles* also frequently use non-richochetal brachiation (Fleagle, 1976; Jenkins et al., 1978; Jungers and Stern, 1984; Mittermeier and Fleagle, 1976; Cant et al., 2003; Usherwood and Bertram, 2003) but there are biomechanical differences between these taxa. *Ateles* uses a prehensile tail during the support phase of brachiation (Richard, 1970; Jenkins et al., 1978; Mittermeier and Fleagle, 1976; Jungers and Stern, 1984) while *Symphalangus* performs a pull-up or hoist during the support phase to elevate the centre of gravity and permit a greater drop and acceleration during the subsequent downswing (Jungers and Stern, 1981; Larson, 1988). *Symphalangus* also employs ricochetal brachiation, characterised by an aerial phase between handholds (Fleagle, 1976; Jungers and Stern, 1984; Cant et al., 2003; Usherwood and Betram, 2003). Both these brachiating modes in *Symphalangus* are likely to increase stress on the humerus relative to *Ateles*.

In contrast to largely terrestrial African apes, the humerus of *Pongo*, *Symphalangus* and *Ateles* is most frequently loaded above the head such that tensile forces are thought to predominate (Swartz et al., 1989; Preuschoft et al., 2010). The main compressive forces are those resulting from muscle contraction alone so that compression load magnitude is lower than that of knuckle-walking *Pan* and *Gorilla* (Carlson and Patel, 2006; Preuschoft et al., 2010). In addition, the irregularity of substrates and superstrates within an arboreal environment requires diverse positioning and loading of the limbs compared to more uniform terrestrial environments (Kimura, 2002; Carlson, 2005).

While non-human primates utilise their humerus in a supportive capacity to bear their mass during locomotion, bipedal humans use the humerus primarily in a manipulative capacity below the shoulder level. Thus, it is likely that the proximal humerus is typically subject to lower magnitude loads (although still high; see Westerhoff et al., 2009b; Bergmann et al., 2011) than would occur during quadrupedal locomotion (Scherf et al., 2013). Furthermore, the typical combination of different manual activities would load the humerus in multiple directions, unless a

particular individual engaged in a highly repetitive, habitual activity (Büchler et al., 2002; Bergmann et al. 2007; Westerhoff et al., 2009a,b; Scherf et al., 2016).

Australopiths were bipedal hominins (e.g., Susman et al., 1984; Stern, 2000; Lovejoy et al., 2002; Ward, 2002, 2013), which would have freed the forelimbs from habitually supporting body mass. However, there is debate regarding the extent to which different australopith species also engaged in arboreal behaviors and thus the extent of humeral loading from locomotion (e.g. Ward, 2002, 2013; Niemitz, 2010). A suite of external skeletal traits, primarily those of the lower limb (e.g., Haeusler 2002; Latimer, 1991; Ward et al., 2011), indicate habitual bipedalism, while morphological features of the upper limb, including the morphology of the humeral head, suggest the potential for use of suspensory and climbing behaviors (Stern and Susman, 1983; Ward, 2002; Toussiant et al., 2003: Arias-Martorell et al., 2015a). *A. africanus* fossils from Member 4 Sterkfontein - from which the specimen in this study derives - exhibit fore-to-hindlimb joint proportions more akin to extant apes than those of modern humans (McHenry and Berger, 1998; Green et al., 2007) and upper limb morphology that retains primitive features of early hominins and/or extant non-human apes (e.g. McHenry, 1983; Toussaint et al., 2003). These morphological features have led some researchers to conclude that arboreal behaviors, and particularly climbing, were an important part of the *A. africanus* locomotor repertoire (McHenry, 1983; McHenry and Berger, 1998; Green et al., 2007). If so, frequent arboreal locomotion would likely result in greater and more varied humeral loading in australopiths than that of modern humans.

Aims and predictions

Our study will build on previous investigations in two ways. Firstly we will incorporate new extant and fossil species into our analyses; our sample includes humans, African and Asian apes, and *Ateles*, of which *Gorilla* and *Ateles* have not been included in previous studies (Ryan and Shaw, 2012; Scherf et al, 2013), and use this comparative sample to investigate the trabecular structure in *A. africanus*. Secondly, we will employ two distinct but comparable methodologies: (1) we apply the traditional VOI-based method of analysing trabecular bone to compare our results directly to

previous studies and (2) we quantify trabecular structure throughout the entire humeral head epiphysis, including visualisation of variation in BV/TV and DA, to highlight potential variation in glenohumeral joint posture during peak loading.

The specific aims of this study are threefold. First (**Aim 1**), we quantify for the first time the trabecular structure throughout the entire proximal epiphysis to investigate the correlation between trabecular structure and inferred differences in joint loading across different locomotor and manipulative behaviors. We predict that variation in trabecular structure will correlate with the habitual loading regime of the humeral head employed by different primates during locomotor or manipulative behaviors. More specifically, we predict that in knuckle-walking taxa (*Pan* and *Gorilla*) where the humeral head is thought to predominantly experience high, stereotypical compressive joint reaction forces arising from both muscle contraction and gravitational forces operating on the supported body mass, DA and BV/TV, as well as trabecular number (Tb.N) and/or trabecular thickness (Tb.Th), will be higher. In contrast, in suspensory taxa (*Pongo*, *Symphalangus* and *Ateles*) where the compressive loads experienced by the humerus are lower (Carlson and Patel, 2006) and more diverse (Kimura, 2002; Carlson, 2005; Michilsens et al. 2012), we expect DA and BV/TV (as well as Tb.N and/or Tb.Th) to be lower. Finally, we assume loading of the human humeral head to be diverse from highly varied manipulative behaviors, and the magnitude lower than the stress incurred during locomotion (both terrestrial and arboreal). Thus, we predict that humans will have low BV/TV, as shown in previous studies (Ryan and Shaw, 2015; Chirchir et al. 2015) and also a more isotropic trabecular structure.

The whole-epiphysis approach allows visualisation of how BV/TV varies throughout the humeral head. Given that bone is deposited at regions of highest mechanical loading (van der Meulen et al., 2006; Barak et al., 2011), we predict that concentrations of BV/TV will reflect joint posture (position of the humeral head relative to the glenoid fossa) at peak loading. Since the precise articular relationships between the humeral head and glenoid fossa during different locomotor behaviors in non-human primates remain largely unexplored [but see, e.g. Soslowsky et al. (1992) and Büchler et al. (2002) for clinical studies of the human humeroglenoid joint and Patel

et al. (2018) for a study of glenoid fossa subchondral bone radiodensity in humans, chimpanzees and gibbons], we predict only that knuckle-walking taxa, suspensory taxa and humans will show greater intra-group similarities than inter-group similarities.

Our second aim (**Aim 2**) is to examine how results from the VOI-based and whole-epiphysis approaches vary and how each correlates with inferred differences in joint loading across different locomotor and manipulative behaviors. Despite potential biases that might arise from quantifying different volumes of trabecular bone (Fajardo and Müller, 2001; Kivell et al., 2011; Scherf et al., 2013), we predict that similar relative differences in trabecular parameters will be found across the different locomotor/manipulative groups in both methods. We also test for allometry in trabecular bone variables following results of previous studies (Ryan and Shaw, 2012, 2013; Barak et al., 2013).

Finally, within this comparative context, our third aim (**Aim 3**) is to elucidate locomotor and/or manipulative behavioral signals in an *A. africanus* (StW 328) partial humerus. Based on previous research showing relatively high BV/TV in hominins compared with recent humans (Chirchir et al. 2015; Ryan and Shaw, 2015), we predict that StW 328 will have high BV/TV compared with our human sample. However, if *A. africanus* still frequently used its forelimbs for arboreal locomotion, the pattern of BV/TV concentration should be more similar to that of arboreal apes than to humans. It is important to note that poor preservation of the lateral and posterior portions of the StW 328 humeral may prohibit revealing a clear trabecular pattern.

MATERIALS AND METHODS

Study sample

Details of the study sample are presented in **Table 1**. Trabecular structure was examined in the humeri of 12 *Pan troglodytes verus,* six *Gorilla gorilla,* eight *Pongo pygmaeus,* three *Symphalangus syndactylus*, four *Ateles* sp., nine *Homo sapiens*, and one *A. africanus* (StW 328). A second *A. africanus* specimen that includes the proximal humerus (StS 7) does not preserve imageable trabecular bone due to the inclusion of bright matrix. The sample sizes of the extant taxa are comparable to

previous studies (Ryan and Shaw, 2012; Scherf et al. 2013), and the *Pongo*, *P. t. verus* and human specimens were included the study by Scherf et al. (2013). All extant non-human primate specimens were wild-caught. The modern human material derived from a cadaveric collection from the Institute for Human Genetics and Anthropology, Friedrich Schiller University (Jena, Germany). Either the left or right humerus was used, depending on the availability of specimens and all specimens were free of signs of pathology or post-mortem damage. All extant specimens were considered adults based on complete external epiphyseal fusion in the humerus and associated skeletal elements. However, this analysis revealed that all of the modern humans retained a slight epiphyseal line within the trabecular structure of the humeral head (see Discussion and Fig. SI1).

High-resolution micro-computed tomography

All specimens were scanned using a high-resolution BIR ACTIS 225/300 micro-computed tomographic industrial scanner housed at the Department of Human Evolution, Max Plank Institute for Evolutionary Anthropology (Leipzig, Germany). All specimens were scanned using an acceleration voltage of 130kV at 100 μA and a 0.25 mm brass filter. Isometric voxel size of the resultant scans ranged from 26-30 microns. Images were reconstructed as 2048 X 2048 pixel, 16-bit TIFF stacks from 2500 projections with three frame averaging. Due to limitation in file size in the whole-epiphysis analysis (see below), image stacks of large ape specimens were resampled to between 45 microns (*Pan*-sized) and 80 microns (male *Gorilla*-sized). We tested the impact of resampling on five specimens by extracting a VOI and resampling it to at least three different voxel sizes. This resulted in minimal changes in BV/TV (standard deviation <0.05), DA (standard deviation <0.06) and Tb.Th (standard deviation <0.03) (see Supplementary Information Table SI1).

Whole-epiphysis analysis of trabecular structure

The whole-epiphysis approach allows for visualisation and quantification of the entire trabecular structure throughout the humeral head via the use of multiple sampling spheres or VOIs. As such,

this method differs from the traditional VOI approach (see below) in quantifying trabecular structure both throughout the entire region (e.g. an average BV/TV for the entire epiphysis) and at any specific point within the anatomical region (e.g., difference in BV/TV between the posterior and anterior regions of the epiphysis). For each scan, the humeral head was isolated from the rest of the bone by cropping the image at the surgical neck, an anatomical region approximately homologous across taxa. Images were segmented into binary format using the Ray Casting Algorithm (RCA) (Scherf and Tilgner, 2009). Trabeculae in the fossil specimen StW 328 were well preserved and thus this specimen was also segmented using the RCA method after small matrix inclusions were removed manually. A test of intraobserver error in segmentation (run five times on one *Gorilla* specimen) resulted in mean BV/TV values differing on average by 1.3%. Trabecular variables in the user-defined humeral head were analysed using a customised, in-house software package called medtool (Pahr and Zysset, 2009a). Steps detailing the morphological filters are described in Pahr and Zysset (2009a) and tested in Gross et al. (2014) but a brief description is as follows (**Fig. 1**). From the segmented image (**Fig. 1a**), the outer surface (boundary between cortex and air; **Fig. 1b**) and inner surface (boundary between cortex and trabeculae; **Fig. 1c**) were defined and used to create cortex only (outer surface minus inner surface; **Fig. 1d**) and trabecular only (segmented image minus cortex only image; **Fig**. **1e**) images. A mask overlay image (**Fig. 1f**) was generated and separate grey values assigned to the cortex, trabecular bone and 'air'. 2D meshes of outer and inner isosurfaces were then created and the cortex and trabecular region volumes filled with tetrahedral finite elements in HyperMesh® (Altair Engineering Inc., USA) (Pahr and Zysset, 2009b). This enabled generation of 3D meshes of these regions (**Fig. 1g)**.

Trabecular thickness (Tb.Th, mm) was calculated from the trabecular only image using the BoneJ plugin (version 1.3.1; [61]) for ImageJ (version 1.46r) (Doube et al., 2010). To quantify BV/TV and trabecular orientation (the second rank fabric tensor), a 5 mm-diameter sampling sphere was placed at each node of a 3D background grid (2.5 mm grid spacing) applied to the 3D trabecular mesh (Gross et al., 2014). Bone volume fraction was calculated as the ratio of bone voxels to bone and air voxels. The second rank fabric tensor is calculated using the mean intercept

length method (Whitehouse, 1974; Odgaard, 1997) and the first, second and third eigenvectors and eigenvalues were extracted. Calculations were made at each node and an average obtained for the entire region. Fabric degree of anisotropy (DA) is calculated as 1 minus eigenvalue 3/eigenvalue 1 and describes trabecular organization or degree of alignment among trabecular struts. Bone density maps, which are visual representations of BV/TV distribution across the defined region, were created in Paraview 3.14.1 (Sandia Corporation, Kitware. Inc). A test of mesh size variation in one specimen revealed differences of less than 1% in calculated BV/TV and DA. Other trabecular variables, such as trabecular number (Tb.N), separation (Tb.Sp) and pattern factor (Tb.Pf), were not able to be quantified within the medtool script (Pahr and Zysset, 2009a).

Volume of interest-based analysis of trabecular variables

In addition to the whole-epiphysis analysis, trabecular structure was quantified using the traditional VOI approach, in which only a subsample of the trabecular structure is analysed within the humeral head (**Fig. 2**). The volume was defined and extracted from each epiphysis in AVIZO 6.3® (Visualization Sciences Group, SAS). To ensure homologous (scaled) size and position, a cubic volume was defined by the maximum and minimum extents of the articular surface in the x, y and z dimensions. The midpoint of the cube's x, y and z dimensions was located and a smaller cubic VOI was extracted from the epiphysis and exported as an image stack (.bmp format). The size of this VOI was calculated as 30% of the geometric mean of the maximum superior-inferior and anterior-posterior dimensions of the articular surface. The VOI image stack was then imported into CTAn® (Skyscan, 2007) for analysis using a spherical volume of interest. In addition to trabecular thickness, BV/TV and DA, which are directly comparable to the same parameters output in the whole-epiphysis analysis, trabecular number (Tb.N, mm^{-1}), trabecular separation (Tb.Sp, mm), and trabecular pattern factor (Tb.Pf, mm^{-1}; an inverse index of connectivity with low Tb.Pf indicating a more highly connected lattice and negative values signifying many enclosed cavities). Details on the calculation of these parameters can be found in Lazenby et al. (2011). Calculation of trabecular parameters is similar across the different software programs; both BoneJ (Doube et al., 2010) and

CTAn® (Skyscan, 2007) calculate Tb.Th based on Hildebrand and Rüegseggar (1997), while both medtool (Pahr and Zysset, 2009a; Gross et al. 2014) and CTAn® (Skyscan, 2007) calculate BV/TV as a ratio of bone voxels to total voxels and DA based on the mean intercept length (Odgaard, 1997). As such, we do not anticipate any inherent bias based on the different programs used.

[INSERT TABLE 1 AND FIGS. 1 & 2 ABOUT HERE]

Statistical analyses

Data for all trabecular variables obtained from both the whole-epiphysis and VOI analyses were tested for allometry in PAST (v. 2.16) using ordinary least squares regression. *Ateles* was excluded from regressions to generate hominoid-only results comparable to those of Ryan and Shaw (2013). Since body size was unavailable for the study sample, the geometric mean of epiphysis size (see above) was used as a proxy for body size.

Due to small sample size and unknown sex for many specimens, all statistical analyses were conducted on the pooled sample of each taxon. Pair-wise comparisons using Kruskal-Wallis tests were used to investigate differences between specific taxa for all variables. Variation in trabecular parameters was depicted graphically with box-and-whisker plots. A principal components analysis (PCA) was conducted in PAST (v. 2.16) to investigate how a suite of trabecular variables may distinguish among different taxa/locomotor groups. The PCA was restricted to the VOI data because more trabecular variables (BV/TV, Tb.N, Tb.Th, Tb.Sp, Tb.Pf, and DA) could be quantified within the VOI compared with that of the whole-epiphysis approach (BV/TV, DA and Tb.Th). The PCA was run on all of the trabecular variables, including BV/TV, and with BV/TV excluded because it was highly correlated with several of these variables. The results of both PC analyses revealed similar relationships among the taxa and thus only the results including all of the trabecular variables are presented here. Due to unequal scale of variables, the PCA was conducted on the correlation matrix rather than on raw variables. Previous analyses have found no significant phylogenetic signal in trabecular structure of the primate humerus (Ryan and Shaw, 2012; Scherf et al., 2013) so this is not investigated here.

RESULTS

Allometry

Ordinary least squares regressions reveal that several variables are significantly correlated with the geometric mean of the humeral head epiphysis size (**Table 2**). Raw and logged Tb.Th (from both the whole-epiphysis and VOI analyses) scaled with negative allometry, indicating a relative thinning of trabecular bone as humeral head size increases. In the VOI, raw and logged Tb.N and Tb.Sp also scale with negative allometry. Logged DA scaled positively but raw DA did not scale significantly.

[INSERT TABLE 2 ABOUT HERE]

Comparison of individual trabecular variables

A coronal cross-section of the trabecular structure of the humeral head in a representative specimen from each extant taxon and *A. africanus* is shown in **Figure 3** (see also Figs. SI1-6 for images of the complete sample). These images show some general trabecular patterns that were common in all taxa. The trabeculae were most dense, highly connected and uniformly oriented close to the articular surface. Trabeculae were also highly connected and uniformly oriented around the sub-cortical region of the surgical neck. In contrast, the central region of the head as it merges into the humeral shaft was characterised by a more isotropic structure with sparse, widely spaced, unconnected trabeculae. This latter pattern was most accentuated in humans, in which some specimens displayed an absence of trabeculae in the central-most region. In *Pan* this pattern was less marked and distribution was more homogenous throughout the entire humeral head. Humans retained a distinct internal epiphyseal line despite presenting with adult morphology externally. These trabecular patterns are further visualised in 3D in the colour maps of trabecular density (see below).

For each trabecular variable from both the whole-epiphysis and VOI approaches, summary statistics are presented in **Table 3** and box-and-whisker plots are shown in **Figure 4**. Results of pairwise comparisons across different taxa for the whole-epiphysis and VOI data are presented in **Table 4**. Kruskal-Wallis tests indicate significant differences in Tb.Th (whole-epiphysis $p<0.001$,

VOI $p<0.001$), BV/TV (whole-epiphysis $p = 0.012$, VOI $p = 0.003$) and DA (whole-epiphysis $p = 0.025$, VOI $p = 0.002$) across all taxa.

In the whole-epiphysis analysis, *Gorilla* had significantly thicker Tb.Th than all other species except *Pongo* (**Table 4**). *Pongo* had significantly thicker trabeculae than smaller-bodied suspensory species *Symphalangus* and *Ateles*. Results from the VOI analysis were similar, with the exception that humans exhibit significantly thicker trabeculae than *Pan*, *Symphalangus* and *Ateles* (humans also had higher Tb.Th than all of these taxa in the whole-epiphysis analysis but this difference was not significant; **Fig. 4**). The *A. africanus* specimen showed similar Tb.Th values to humans in the whole-epiphysis but had lower Tb.Th values derived from the VOI and, in this way, was most similar to *Symphalangus* and *Ateles*.

BV/TV in the whole-epiphysis was highest in *Pan* and *Gorilla* and lowest in humans, with significant differences between *Pan*-humans and *Gorilla*-humans (**Table 4**). Suspensory *Pongo, Symphalangus* and *Ateles* were intermediate between African apes and humans. The VOI analysis yielded similar results; BV/TV is highest in *Pan* and *Gorilla* and both were significantly higher than *Pongo*, *Ateles*, and humans. *A. africanus* had relatively high BV/TV in the whole-epiphysis analysis, falling in between *Gorilla* and *Symphalangus*, but had the lowest BV/TV of the study sample in the VOI analysis, falling closest to humans (**Table 3**).

Humans, *Gorilla* and *Pan* demonstrated the highest DA in the whole-epiphysis analysis, while *Ateles* and *Symphalangus* had the lowest DA (**Fig. 4**). Humans were significantly higher than all suspensory taxa, while both *Gorilla* and *Pan* were significantly higher than *Ateles* only (**Table 4**). *Pongo* had DA values that were intermediate relative to the remainder of the study sample. DA values derived from the VOI were also high in *Pan* and *Gorilla*, and low in *Ateles* and *Symphalangus*. Differences are significant between *Pan*-humans, *Pongo*-humans, *Pan-Symphalangus, Pan-Ateles* and *Gorilla-Symphalangus*. However, in contrast to the results from the whole-epiphysis, *Pongo* had the highest DA, close to the values of *Pan* and *Gorilla*. Although the DA values for humans were similar between both analyses, the relative values across the remaining sample differed (**Fig. 4**). As such, humans had significantly lower VOI DA values than *Pan*, *Gorilla* and *Pongo,* which contrasts

with the whole-epiphysis results (**Table 4**). *A. africanus* had relatively low DA in both analyses, falling out most similar to *Pongo* in the whole-epiphysis and most similar to *Ateles* and humans in the VOI analysis (**Table 3**).

[INSERT TABLES 3 & 4 AND FIGS. 3 & 4 ABOUT HERE]

Bone volume fraction and degree of anisotropy in the whole-epiphysis

A bivariate plot of DA against BV/TV, as quantified in the whole-epiphysis, revealed substantial overlap across taxa, but a pattern that generally distinguishes different behavioral categories (**Fig. 5**). Knuckle-walking *Pan* and *Gorilla* were generally distinguished from suspensory taxa in having higher DA and BV/TV. Humans displayed a wide range of variation but were broadly distinguished from knuckle-walkers and suspensory taxa in having very low BV/TV but higher DA. Suspensory taxa fell out as intermediate between knuckle-walkers and humans in BV/TV but with generally lower DA, especially in *Ateles* and *Symphalangus*. *A. africanus* fell within the overlapping ranges of the great apes and modern humans for both BV/TV and DA. However, it exhibited higher BV/TV than all but one human and its DA was higher than that of most suspensory specimens (**Fig. 5**).

Distribution of bone volume fraction throughout the humeral head

Colour maps of the distribution of BV/TV throughout the humeral head are shown for one representative specimen of each of the extant taxa in **Figure 6** and *A. africanus* in **Figure 7**. Colour maps for the entire sample are shown in the Supplementary Information Figures SI1-6. Visualisation of BV/TV distribution confirmed the taxonomic variation in trabecular patterns noted above in the segmented coronal cross-sections (**Fig. 3**). The colour maps further revealed that BV/TV is highest (>40%) medially, in the sub-articular region of the humeral head in all specimens, although both the degree and the precise axial location varied across taxa.

When all specimens were scaled to the same BV/TV range (0-45%; **Fig. 6**), *Pan* and *Gorilla* demonstrated the largest regions of high BV/TV and a coronal midslice revealed that these high-

density regions penetrate further into the centre of the humeral head than in all other species. In *Pan* the regions of lowest density (<10% BV/TV) were minimal or absent, demonstrating a more uniform distribution of BV/TV than that of *Gorilla*. Both species show a medial, slightly superior but largely posterior concentration of trabecular bone. *Gorilla* specimens exhibited a more localised, parasagittally-oriented band of highest concentration from the posterior to the superior region of the articular surface that was not as evident in *Pan* (see also Figs. SI2-3).

Among the suspensory taxa, a coronal midslice of the *Pongo* humeral head revealed a superior concentration of high BV/TV. *Ateles* and *Symphalangus*, on the other hand, exhibited a more medio-posterior concentration. *Symphalangus* demonstrated higher BV/TV throughout the humeral head compared with *Pongo* and *Ateles* (**Fig. 6**).

In humans, the BV/TV concentration was largely confined to the sub-articular region, barely penetrating into central regions of the humeral head. Several modern human specimens had large areas of BV/TV of less than 10%. Coronal midslice images showed a localised superior concentration in modern humans (**Fig. 6**).

Although the StW 328 *A. africanus* humeral head was not complete, trabecular structure within the preserved portion of the humeral head is intact (**Fig. 7**). Maximum BV/TV was confined to the sub-articular surface, similar to the pattern seen in humans. However, the regions of lowest BV/TV (<10%) were smaller than in humans. It was not possible to determine the precise pattern and extent of the highest BV/TV concentration due to incompleteness (**Fig. 7**).

[INSERT FIGS. 6 & 7 ABOUT HERE]

Principal components analysis on volume of interest data

Figure 8 shows the results of a PCA using five trabecular parameters derived from a VOI. The first two principal components accounted for 79.8% of the total variance. Along the first principal component (PC1) (47.9%), *Gorilla*, *A. africanus* and most humans and *Pongo* were distinguished from *Pan, Symphalangus* and *Ateles*, in having lower Tb.N and greater Tb.Sp (**Table 5; Fig. 8**). Along

PC2 (31.9%), *Gorilla* was mainly distinguished from all other taxa in having higher Tb.Th and BV/TV and a more anisotropic trabecular structure, although several human, *Pongo* and *Pan* specimens overlap with the *Gorilla* distribution. Despite overlap, there was generally sufficient distinction among taxa to describe a characteristic trabecular structure but this did not hold true for locomotor categories.

Systematic comparison of whole-epiphysis and VOI results

In addition to the individual variables that differ across species in the whole-epiphysis and VOI-based results (**Table 4**), there were notable systematic differences within each taxon for each variables (**Table 3; Fig. 4**). Mean values for Tb.Th were generally higher across all taxa in the VOI analysis compared with the whole-epiphysis results. This was especially the case in humans, with Tb.Th 27.0% higher in the VOI analysis than the whole-epiphysis analysis (**Table 3**). However, *Pongo* and, more markedly, *A. africanus* were exceptions, both showing higher Tb.Th values (by 4.3% and 16.4% respectively) in the whole-epiphysis analysis than the VOI result. Mean values of BV/TV and DA were also systematically higher within each taxon in the VOI analysis than in the whole-epiphysis analysis. *A. africanus* was the only exception with a much higher (45.2%) BV/TV value in the whole-epiphysis analysis. Although the VOI analysis generally yielded systemically higher values for all variables than the whole-epiphysis analysis in each of the extant taxa, the degree of this increase was not consistent across taxa for any variable. For example, *Gorilla* BV/TV was 28.6% higher in the VOI in the whole-epiphysis analysis, but *Pongo* BV/TV was only 1.8% higher.

[INSERT TABLE 5 AND FIG. 8 ABOUT HERE]

DISCUSSION

This study investigated the relationship between trabecular structure and loading regime in the humeral head of several primate taxa and *A. africanus*. Our aims were (1) to quantify for the first time the trabecular structure throughout the entire proximal epiphysis in order to investigate

1 the correlation between trabecular structure and inferred differences in joint loading across
2 different locomotor and manipulative behaviors; (2) to examine how results from the traditional
3 VOI-based methods compare to that of the whole-epiphysis analysis; and (3), within this
4 comparative context, elucidate locomotor and/or manipulative behavioral signals in the *A.*
5 *africanus* StW 328 partial humerus.
6
7 ***Allometry***
8 The allometric relationship between different trabecular parameters and humeral epiphysis size
9 was similar to that found in previous studies of the primate humerus in a more diverse primate
10 sample (Ryan and Shaw, 2013) and to studies of other skeletal elements (Cotter et al., 2009;
11 Fajardo et al., 2013) and broader mammalian samples (Doube et al., 2011; Barak et al., 2013).
12 Trabecular thickness, spacing and number scaled with negative allometry, indicating that smaller
13 primates have relatively thicker, more separated and more numerous trabeculae than in larger
14 primates (Ryan and Shaw, 2013). However, unlike Ryan and Shaw (2013), we found that the
15 relationship between BV/TV and the size of humeral epiphysis was not significant (rather than
16 positively allometric) and that DA showed weak positive allometry. Other studies have also found
17 BV/TV and DA to be (largely) independent of body mass across several primate species (Cotter et
18 al., 2009; Fajardo et al., 2013) and mammal species (Doube et al., 2011; Barak et al., 2013). This
19 may be due to differences in the respective study samples (i.e., range of taxa and body size),
20 variation in trabecular scaling across different skeletal elements, and/or differences in
21 methodology. Furthermore, phylogenetically informed linear regressions indicate that scaling
22 relationships may vary between primate taxa (Ryan and Shaw, 2013), as is the case in rodents and
23 humans (Barak et al., 2013). As such, to accurately determine scaling relationships of trabecular
24 structure, regression analyses should be conducted on a taxon-specific basis, rather than across
25 broad taxonomic groups. However, obtaining large enough sample sizes of high-resolution CT data
26 to test within-species allometry remains challenging.
27

Does trabecular structure distinguish behavioral modes and loading regime?

To address Aim 1, we predicted that DA and BV/TV, as well as Tb.N and/or Tb.Th (which are correlated with BV/TV) would be higher in knuckle-walking taxa in which the humerus is thought to most frequently experience higher and more stereotypical compressive loading. We also predicted that suspensory taxa would show the opposite pattern due to lower and more diverse loading of the proximal humerus. Finally, we expected that humans would have the lowest BV/TV values, consistent with previous research (e.g. Scherf et al. 2013; Chirchir et al. 2015; Ryan and Shaw, 2015), and predicted low DA due to the low magnitude and diverse loading assumed to occur during manipulative activities. In general, the results from both whole-epiphysis and VOI-based analyses supported these predictions.

The results of both the whole-epiphysis and VOI analyses in this study largely concurred with previous studies of humeral head trabecular structure (Ryan and Shaw, 2012; Scherf et al., 2013), finding separation between knuckle-walking *Pan* and suspensory *Pongo*, and that the trabecular structure of humans overlapped more with *Pongo* than with *Pan*. As predicted, we found that most knuckle-walking individuals displayed higher BV/TV, Tb.Th and DA than most suspensory individuals, with *Ateles* and *Symphalangus* being particularly distinct. Humans were generally distinct from all other taxa, due largely to the lowest BV/TV values in both types of analyses, and showed relatively low DA that was more similar to suspensory taxa than to knuckle-walking taxa in the VOI analysis, supporting our predictions (see below). Therefore, VOI-based analyses [including Ryan and Shaw (2012) and Scherf et al. (2013)] and, to a lesser degree, whole-epiphysis analyses show that analysis of several aspects of trabecular structure together (e.g. BV/TV, DA, Tb.Th) can distinguish, to some extent, among species with different locomotor repertoires. However, there was considerable overlap in our sample across locomotor and taxonomic groups and analyses of different trabecular variables revealed that the overall structure was not the same across taxa in any given behavioral group.

Pan and *Gorilla* both exhibited high BV/TV, DA and low Tb.Pf (highly connected trabeculae), as predicted, but the overall trabecular structure was not the same. *Pan* trabeculae were more

numerous and closely packed (i.e., higher Tb.N and lower Tb.Sp); a trabecular pattern also reported in *Pan* by previous studies of the humerus (Ryan and Shaw, 2012; Scherf et al., 2013) and vertebrae (Liu et al., 2009). In contrast, *Gorilla* had significantly higher Tb.Th than *Pan*, suggesting that different trabecular parameter combinations may result in similar mechanical properties. These results make clear that not all knuckle-walkers have the same trabecular structure and highlight the importance of including more than just *Pan* in a comparative sample.

In both the whole-epiphysis and VOI analyses, suspensory taxa *Pongo, Symphalangus* and *Ateles* all demonstrated lower BV/TV (though this difference was not significant in *Symphalangus*) and higher Tb.Pf (less connected trabeculae) than that of knuckle-walking taxa. This result is consistent with previous findings of a less compact structure in *Pongo* (Ryan and Shaw, 2012; Scherf et al, 2013). Contrary to our predictions, *Symphalangus*, *Ateles* and, to a lesser degree, *Pongo*, shared high Tb.N and low Tb.Sp (i.e., more numerous and closely-packed trabecular structure) with *Pan* (**Table 3; Figs. 4 and 8**). All suspensory taxa also showed lower DA than knuckle-walking taxa, in the whole-epiphysis and VOI analyses, supporting our prediction of more diverse loading of the proximal humeral joint in the former group. The notable exception to this was the high DA value for *Pongo* in the VOI analysis, which was significantly higher than other suspensory taxa and humans and more similar to African apes (**Fig. 4**). This VOI result is consistent with the results of Scherf et al. (2013), which also used a VOI-based analysis. These varying results suggest that particular regions (in this case, the more central region of the epiphysis) of the *Pongo* proximal humerus may be relatively anisotropic but that the overall structure throughout the epiphysis is more isotropic like other suspensory taxa. This more anisotropic structure in *Pongo* may reflect allometry, as we found a weak positive relationship between DA and body mass, or it may relate to functional reasons that are currently unclear.

In the whole-epiphysis analysis, the mean BV/TV value for humans was lower than that of all other taxa, and significantly so compared to knuckle-walking taxa. Humans demonstrated a sparse structure with few, relatively unconnected trabeculae consistent with previous analyses of humans (Ryan and Shaw, 2012, 2015; Scherf et al., 2013; Chirchir et al., 2015). In the VOI analysis, the

human BV/TV was relatively higher, being more similar to suspensory taxa (but still significantly lower than knuckle-walking taxa). Results for DA in humans also contrasted between the two approaches. In the whole-epiphysis analysis, humans had significantly more anisotropic trabeculae than *Pongo*, *Ateles* and *Symphalangus* and mean values were higher than those of knuckle-walkers. Scherf et al. (2013) reported an even higher mean DA for humans quantified from VOIs. However, in our VOI analysis, human DA was significantly lower than that of knuckle-walkers and *Pongo*. Overall, these DA results did not support our predictions and, together with the DA results in *Pongo*, demonstrate that DA values are particularly dependent on the method used (see below).

Does the distribution of bone volume fraction reflect joint posture?

The whole-epiphysis analysis enabled visualisation of BV/TV variation throughout the entire humeral head, helping to address our first aim of investigating the correlation between trabecular structure and inferred joint loading (**Fig. 6** and **Figs. SI1-6**). In all taxa, BV/TV was highest at the subarticular surface where forces are initially incurred, and there were greater similarities in the distribution of high BV/TV across the taxa than was initially predicted.

Pan and *Gorilla* showed the largest concentrations of high BV/TV that penetrated much further into the epiphysis than in any other taxa. This pattern is consistent with the quantitative results described above and generally high compressive loading of the humerus during knuckle-walking. However, high BV/TV was distributed within the medio-posterior and superior aspects of the humeral head, which is not consistent with a more anterior humeral head-glenoid contact that would be expected during protraction and retraction of the humeral head during knuckle-walking (Hunt, 1991b, 1992; Inouye, 1994). Instead, the BV/TV pattern found in African apes is more similar to that of the suspensory taxa and may reflect arboreal behaviors, particularly climbing. We did not predict a functional signal of an arboreal (i.e., above-the-shoulder) arm posture in African apes given their high frequency of quadrupedal knuckle-walking. However, both species, and particularly *Gorilla*, may engage in more frequently in arboreal locomotor behaviors than previously thought (Crompton et al., 2010). That being said, *Gorilla* showed a parasagittal band of

high BV/TV that extended more anteriorly than was found in *Pan*, which may be consistent with more frequent parasagittal protraction and retraction of the humerus during knuckle-walking (Tuttle and Watts, 1985; Hunt, 1991a; see Figs. SI2-3). Arthrokinematic data on shoulder joint posture in *Pan* and *Gorilla* during knuckle-walking and different types of arboreal locomotion are needed to clarify the peak loading postures of the glenoid fossa and humeral head to fully interpret the similarities and differences in distribution of BV/TV in both of these taxa.

Pongo displayed a superior concentration of BV/TV, consistent with abduction or flexion of the humerus to shoulder level and above. As the humerus is elevated, the superior region of the head articulates with the glenoid fossa (Soslowsky et al., 1992; Arias-Martorell et al., 2015b). Elevation above shoulder level causes superior orientation of the scapula, including the glenoid fossa, and thus the same region of articulation is maintained (Soslowsky et al., 1992). This solely superior concentration was absent in *Ateles* and *Symphalangus*; instead they showed a medio-superior distribution of high BV/TV. This difference possibly reflects different joint postures during brachiation and slow orthograde clambering (Fleagle, 1976; Cant et al., 2001). Further variation in trabecular patterns found between *Symphalangus* and *Ateles*, particularly larger regions of higher BV/TV in *Symphalangus*, may reflect the use of quick, ricochetal brachiation (Fleagle, 1976; Jungers and Stern, 1981; 1984; Cant, 2003), a pull-up phase during non-ricochetal braciation (Jungers and Stern, 1981, Larson, 1988) and the absence of a prehensile tail, all which may increase loading at the glenohumeral joint.

Conversely, similar BV/TV distributions may result from distinct joint postures. Both *Pongo* and humans exhibited a superior concentration of BV/TV. In *Pongo*, this likely reflects use of the arms in suspensory, abducted postures at or above the level of the shoulder. While humans generally engage in manipulative behaviors predominantly below shoulder level (Westerhoff et al. 2009b; Scherf et al. 2016), it may be only those at or above shoulder level (during which articulation is superior; Soslowsky et al. 1992) that incur loads great enough for increased bone deposition and subsequent increases in BV/TV. This is supported by empirical data reporting maximum forces during above the shoulder activities (Bergmann et al., 2011). The similar

distributions in *Pongo* and humans may also be related to the requirement in both species for highly mobile glenohumeral joints, for diverse arboreal behaviors (orthograde clambering on irregular substrates/superstrates) and irregular manipulative behaviors, respectively. This is also consistent with the high BV/TV in the superior region of the *Pan* and *Gorilla* proximal humerus, as African apes also require highly mobile glenohumeral joints for arboreal locomotion.

Large regions of BV/TV under 10% in humans support our prediction that habitual loading of the proximal humerus is lower than in non-human primates. This may help to explain the retention of a faint epiphyseal line, wherein loading does not attain magnitudes sufficient to completely remodel this structure. However, recent studies have shown a systemic pattern of low BV/TV in throughout the skeleton of recent sedentary humans (Chirchir et al., 2015; Ryan and Shaw, 2015), including skeletal elements that incur high loads due to bipedalism, such as the femoral head (Ryan and Shaw, 2012), vertebrae (Cotter et al., 2009) and calcaneus (Maga et al., 2006). As such, there may be a taxon-specific systemic pattern to trabecular structure throughout the skeleton and low BV/TV in the human humeral head may not solely reflect loading intensity (Tsegai et al. 2018).

Comparison of whole-epiphysis and VOI results

The second main aim of this study was to examine variation in results derived from two different approaches to measuring trabecular structure: the whole-epiphysis analysis and VOI analysis. We found notable differences in trabecular parameter results for specific taxa and the two approaches yielded systematic differences across taxa and variables, which did not support our prediction.

Broadly, results from the VOI yielded higher values for the Tb.Th, BV/TV and DA within most taxa than the whole-epiphysis approach. In some cases, this difference was minimal (e.g. Tb.Th and BV/TV values in *Pan* and all suspensory taxa), while in other taxa the variables showed a much greater discrepancy. In particular, all DA values derived from the VOI were substantially higher within all taxa, except humans, than those derived from the whole-epiphysis. This difference was most striking in *Pongo*, in which the whole-epiphysis approach yielded a relatively low DA value (mean 0.129), similar to other suspensory taxa and supporting our predictions based on diverse

loading direction during arboreal behaviors. In contrast, the VOI yielded a much higher DA value (mean 0.293) in *Pongo* that was similar to that of African apes. Scherf et al. (2013) also predicted low DA in the *Pongo* humerus but found even higher DA values using a larger and more superiorly-placed VOI. This discrepancy in DA between the two methods is consistent with the findings of Kivell et al. (2011) that DA values are particularly susceptible to changes in VOI location in the hand bones (but relatively robust to changes in VOI size). Thus, the differing results found in this study likely reflect variation in the location of the trabeculae being quantified. In other words, certain regions of the humeral proximal epiphysis – in particular, the central region (measured in this study) and central-superior region (measured in Scherf et al., 2013) – have more aligned (anisotropic) trabeculae than other regions. This anisotropy is captured in the VOI analyses but not when trabecular structure throughout the whole-epiphysis is quantified. For example, the differing results in *Pongo* suggest that trabeculae in the superior-central region is substantially more aligned, which may suggest that peak loading of the humerus occurs superiorly when the arm is loaded above the shoulder. Overall, however, the trabecular structure of the entire epiphysis is relatively isotropic, consistent with resisting loads from multiple directions.

In contrast to the remaining sample, human DA results were very similar between the two methods. This may reflect the much lower density of trabeculae in the human epiphysis, such that the central-distal region of the humeral head was essentially empty (**Figs. 3 and 6**) compared with the more "full" and homogeneous trabecular distribution in our non-human primate sample. As such, in humans there is less trabeculae being quantified in the whole-epiphysis analysis and what was quantified by the VOI is more representative of the overall alignment of the trabeculae throughout the head. The same explanation may apply to variation seen in the results of Tb.Th in both humans and *Gorilla*, such that the VOI yielded higher Tb.Th values than the whole-epiphysis method. Both taxa show the most distinct contrast in BV/TV between the subarticular region of the humeral head, which is extremely dense, and the central region, which is almost empty of trabeculae (**Fig. 6**). Thus, differences between the two methods are increased when the trabecular structure is less homogeneous.

Overall, each method provides different, and potentially functionally relevant, information about loading of the humerus and either method may be valid in future studies depending on the question being addressed. Furthermore, despite the systematic variation across the results, the relative relationships across most taxa/behavioral groups remained the same. For example, *Gorilla*, *Pongo* and humans had the highest Tb.Th using both methods, and knuckle-walking taxa consistently had higher BV/TV than suspensory taxa, and humans always had the lowest BV/TV values. These results are also consistent with previous analyses that have demonstrated minimal phylogenetic influence on trabecular structure in the primate humerus and other skeletal elements (Shaw and Ryan, 2012; Tsegai et al., 2018). However, it is important to note that these species differences were not always statistically significant in both analyses. Thus, when comparing results across studies, it is important to recognise that a VOI-based analyses may provide systematically higher values (depending on VOI placement) for certain trabecular variables than whole-epiphysis-based analyses, and that these differences are likely accentuated in taxa with less homogenous trabecular structure. As such it is necessary to consider relative differences across taxa/behavioral groups rather than rely on statistically significant results alone.

A. africanus *and implications for fossil hominins*

Visualisation and quantification of the trabecular structure in *A. africanus* StW 328 for the first time provides a novel opportunity to glean new functional information about behavior in this fossil taxon and shed light on the debate surrounding the degree of arboreality in australopiths (Stern, 2000; Ward 2002, 2013; Niemitz, 2010; Arias-Martorell et al., 2015a). The correlations between BV/TV distribution and inferred joint posture in extant taxa found here can help to reconstruct joint posture and loading in StW 328, thus addressing our final aim. However, given the variation in the results derived from both methods, we focus on the relative differences between extant taxa and employ caution in making functional inferences. In the VOI analysis, *A. africanus* was similar to humans in having relatively few, widely-separated trabeculae and low BV/TV, suggesting low loading conditions. However, the trabecular structure was highly connected, similar to *Pan*, *Gorilla*

and *Pongo*, which would enable resistance to high loads perhaps associated with arboreal behaviors. Furthermore, the whole-epiphysis analysis showed that *A. africanus* had high BV/TV like that of non-human hominoids suggesting greater loading of the humerus than humans, and possibly some degree of arboreality. Although, it is important to note the low BV/TV in humans is likely systemic and a relatively recent phenomenon; modern human foragers have BV/TV values that are similar to other primates for their body size (Ryan and Shaw, 2015) and thus high BV/TV in *A. africanus* is not inconsistent with a non-arboreal lifestyle. *A. africanus* DA was intermediate between *Pan* and *Pongo* in the whole-epiphysis analysis and similar to *Symphalangus* and *Ateles* in the VOI analysis, suggesting diverse loading the humeral head, perhaps in an arboreal context. Unfortunately, the preservation of the specimen prevents delineation of joint posture on the basis of BV/TV distribution (**Fig. 7**). Although represented by only a single specimen, the preserved trabecular structure of the *A. africanus* proximal humerus is broadly similar to humans, with some structural characteristics that indicate higher, more varied loading possibly reflecting the retention of arboreal locomotion.

The results of this and previous studies make clear that there is variation in primate humeral trabecular structure that correlates with species and, less clearly, locomotor differences, that may help reconstruct behavior in fossil taxa. Greater knowledge of glenohumeral joint posture during maximal loading, particularly in non-human primates, as well as a better understanding of how different trabecular parameters may respond to mechanical stress, are needed to provide further insight into the potential functional signals of humeral trabecular bone. In the short term, application of different trabecular methodologies to larger and broader study samples may help to provide more accurate functional interpretations of variation in trabecular patterns.

ACKNOWLEDGEMENTS

For scanning assistance we thank Heike Scherf and Heiko Temming. For access to specimens in their care we thank Frieder Mayer (Berlin Museum für Naturkunde), Horst Bruchhaus (Friedrich Schiller University), Christophe Boesch (Max Planck Institute for Evolutionary

Anthropology), Bernard Zipfel (Evolutionary Studies Institute, University of Witwatersrand), and Gerhard Haszprunar (Zoologische Staatsammlung München). StW 328 was scanned as part of a collaborative project between the Evolutionary Studies Institute, University of the Witwatersrand and the Department of Human Evolution, Max Planck Institute for Evolutionary Anthropology. We are grateful to Julia Arias-Martorell for helpful comments on an earlier draft of this manuscript and to the Associate Editor and four anonymous reviewers for the insightful suggestions. This study was funded in part by the Max Planck Society (MMS, JJH and TLK) and European Research Council Starting Grant #336301 (MMS, TLK).

REFERENCES

Arias-Martorell J, Potau JM, Bello-Hellegouarch G, Perez-Perez A. 2015a. Like father, like son: assessment of the morphological affinities of A.L. 288-1 (*A. afarensis*), Sts 7 (*A. africanus*) and Omo 119-73-2718 (*Australopithecus* sp.) through a three-dimensional shape analysis of the shoulder joint. PLoS ONE 10: e0117408.

Arias-Martorell J, Tallman M, Potau JM, Bello-Hellegouarch G, Perez-Perez A. 2015b. Shape analysis of the proximal humerus in orthograde and semi-orthograde primates: correlates of suspensory behavior. Am J Prim 77: 1-19.

Barak MM, Lieberman DE, Hublin J-J. 2011. A Wolff in sheep's clothing: Trabecular bone adaptation in response to changes in joint loading orientation. Bone 49: 1141-1151.

Barak MM, Lieberman DE, Hublin J-J. 2013. Of mice, rats and men: Trabecular bone architecture in mammals scales to body mass with negative allometry. J Struct Biol 183:123-131.

Bergmann G, Graichen F, Bender A, Rohlmann A, Halder A, Beier A, Westerhoff P. 2011. In vivo gleno-humeral joint loads during forward flexion and abduction. J Biomech 44:1543-1552.

Bergmann G, Graichen F, Bender A, Kääb M, Rohlmann A, Westerhoff P. 2007. *In vivo* glenohumeral contact forces – measurements in the first patient 7 months postoperatively. J Biomech 40:2139–2149.

Bertram JEA, Swartz SM. 1991. The "law of bone transformation": a case of crying Wolff? Biol Rev Camb Philos Soc 66:245-273.

Biewener AA, Fazzalari NL, Konieczynski DD, Baudinette RV. 1996. Adaptive changes in trabecular architecture in relation to functional strain patterns and disuse. Bone 19:1–8.

Büchler P, Ramaniraka NA, Rakotomanana LR, Iannotti JP, Farron A. 2002. A finite element model of the shoulder: application to the comparison of normal and osteoarthritic joints. Clinical Biomech 17:630-639.

Cant JGH. 1987. Positional behavior of female Bornean orangutans (*Pongo pygmaeus*). Am J Primatol 12:71–90.

Cant JGH, Youlatos D, Rose MD. 2001. Locomotor behavior of *Lagothrix lagothricha* and *Ateles belzebuth* in Yasuní National Park, Ecuador: general patterns and nonsuspensory modes. J Hum Evol 41:141-166.

Cant JGH, Youlatos D, Rose MD. 2003. Suspensory locomotion of *Lagothrix lagothricha* and *Ateles belzebuth* in Yasuní National Park, Ecuador. J Hum Evol 44:685-699.

Carlson KJ. 2005. Investigating the form-function interface in African apes: Relationships between principal moments of area and positional behaviors in femoral and humeral diaphyses. Am J Phys Anthropol 127:312–334.

Carlson K, Lublinsky S, Judex S. 2008. Do different locomotor modes during growth modulate trabecular architecture in the murine hind limb? Integr Comp Biol 48:385–393.

Carlson KJ, Patel BA. 2006. Habitual use of the primate forelimb is reflected in the material properties of subchondral bone in the distal radius. J Anat 208:659–670.

Chirchir H, Kivell TL, Ruff CB, Hublin J-J, Carlson KJ, Zipfel B, Richmond BG. 2015. Recent origin of low trabecular bone density in modern humans. Proc Natl Acad Sci USA 112:366-371.

Cowin SC, Hart RT, Balser JR, Kohn DH. 1985. Functional adaptation in long bones: Establishing in vivo values for surface remodeling rate coefficients. J Biomech 18:665-684.

Cotter MM, Simpson SW, Latimer BM, Hernandez CJ. 2009. Trabecular microarchitecture of hominoid thoracic vertebrae. Anat Rec 292:1098–1106.

Crompton RH, Sellers WI, Thorpe SKS. 2010. Arboreality, Terrestriality and Bipedalism. Philos Trans R Soc Lond B 365: 3301–3314.

Currey JD. 2002. Bones: Structure and Mechanics. Princeton: Princeton University Press.

Doran DM. 1997. Ontogeny of locomotion in mountain gorillas and chimpanzees. J Hum Evol 32:323-344.

Doube M, Kłosowski MM, Arganda-Carreras I, Cordelière FP, Dougherty RP, Jackson JS, Schmid B, Hutchinson JR, Shefelbine SJ. 2010. BoneJ: free and extensible bone image analysis in ImageJ. Bone 47:1076-1079.

Doube M, Kłosowski MM, Wiktorowicz-Conroy A, Hutchinson JR, Shefelbine SJ. 2011. Trabecular bone scales allometrically in mammals and birds. Proc R Soc Lond B Biol Sci. Doi: 10.1098/rspb.2011.0069.

Eriksen EF. 2010. Cellular mechanisms of bone remodelling. Rev Endocr Metab Disord 11:219–227.

Fajardo RJ, DeSilva JM, Manoharan RK, Schmitz JE, MacLatchy LM, Bouxsein ML. 2013. Lumbar vertebral body bone microstructural scaling in small to medium-sized strepsirhines. Anat Rec 296:210-226.

Fajardo RJ, Müller R. 2001. Three-dimensional analysis of non- human primate trabecular architecture using micro-computed tomography. Am J Phys Anthropol 115:327–336.

Fleagle JG. 1976. Locomotion and posture of the Malayan siamang and implications for hominoid evolution. Folia Primatol 26:245–269.

Fox JC, Keaveny TM. 2001. Trabecular eccentricity and bone adaptation. J Theor Biol 212:211–221.

Green DJ, Gordon AD, Richmond BG. 2007. Limb-size proportions in *Australopithecus afarensis* and *Australopithecus africanus*. J Hum Evol 52:187-200.

Gross T, Kivell TL, Skinner MM, N. Huynh Nguyen, Pahr DH. 2014. A CT-image-based method for the holistic analysis of cortical and trabecular bone. Paleontol Electron 17:A17333.

Haeusler M. 2002. New insights into the locomotion of *Australopithecus africanus* based on the pelvis. Evol Anthropol 11:53-57.

Hanna JB, Schmitt D. 2011. Locomotor energetics in primates: gait mechanics and their relationship to the energetics of vertical and horizontal locomotion. Am J Phys Anthropol 145:43-54.

Hanna JB, Schmitt D, Griffin TM. 2008. The energetic cost of climbing in primates. Science 320:898.

Havill LM, Allen MR, Bredbenner TL, Burr DB, Nicolella DP, Turner CH, Warren DM, Mahaney MC. 2010. Heritability of lumbar trabecular bone mechanical properties in baboons. Bone 46:835–840.

Hildebrand T, Rüegsegger P. 1997. A new method for the model-independent assessment of thickness in three-dimensional images. J Microscopy 185:67-75.

Holloway RL. 1980. Within-species brain-body weight variability: a reexamination of the Danish data and other primate species. Am J Phys Anthropol 53: 109-121.

Huiskes R, Ruimerman R, van Lenthe GH, Janssen JD. 2000. Effects of mechanical forces on maintenance and adaptation of form in trabecular bone. Nature 405:704–706.

Hunt KD. 1991a. Positional behavior in the Hominoidea. Int J Primatol 12:95-118.

Hunt KD. 1991b. Mechanical implications of chimpanzee positional behavior. Am J Phys Anthropol 86:521-536.

Hunt KD. 1992. Positional behavior of *Pan troglodytes* in the Mahale Mountains and Gombe Stream National Parks, Tanzania. Am J Phys Anthropol 87:83-105.

Hunt KD, Cant JGH, Gebo DL, Rose MD, Walker SE, Youlatous D. 1996. Standardized descriptions of primate locomotor and postural modes. Primates 37:363-387.

Inouye SE. 1994. The ontogeny of knuckle-walking behavior and associated morphology in the African apes. PhD Dissertation, Northweastern University, Illinois.

Jenkins FA, Dombrowski PJ, Gordn EP. 1978. Analysis of the shoulder in brachiating spider monkeys. Am J Phys Anthropol 48:65-76.

Jungers WL, Stern JT. 1981. Preliminary electromyographical analysis of brachiation in gibbon and spider monkey. Int J Primatol 2:19-33.

Jungers WL, Stern JT. 1984. Kinesiological aspects of brachiation in lar gibbons. In: Preuschoft H, Chivers DJ, Brokelman WY, Creel N, editors. The Lesser Apes: Evolutionary and Behavioral Biology. Edinburgh: Edinburgh University Press. p 119-134.

Kabel J, van Rietenbergen B, Odgaard A, Huiskes R. 1999a. Constitutive relationships of fabric, density, and elastic measures in cancellous bone architecture. Bone 25:481-486.

Kabel J, van Rietenbergen B, Odgaard A, Huiskes R. 1999b. Connectivity and the elastic properties of cancellous bone. Bone 24:115-120.

Kimura T. 2002. Primate limb bones and locomotor types in arboreal or terrestrial environments. Z Morph Anthrop 83:201-219.

Kivell TL. 2016. A review of trabecular bone functional adaptation: what have we learned from trabecular analyses in extant hominoids and what can we apply to fossils? J Anat 228:569-594.

Kivell TL, Skinner MM, Lazenby R, Hublin J-J. 2011. Methodological considerations for analyzing trabecular architecture: an example from the primate hand. J Anat 218:209-225.

Lambers FM, Koch K, Kuhn G, Ruffoni D, Weigt C, Schulte FA, Müller R. 2013. Trabecular bone adapts to long-term cyclic loading by increasing stiffness and normalization of dynamic morphometric rates. Bone 55:325–334.

Lanyon LE. 1974. Experimental support for the trajectorial theory of bone structure. J Bone Joint Surg Br 56:160-166.

Larson SG. 1988. Subscapularis function in gibbons and chimpanzees: Implications for interpretation of humeral head torsion in Hominoids. Am J Phys Anthropol 76:449-462.

Larson SG, Stern JT Jr. 2013. Rotator cuff muscle function and its relation to scapular morphology in apes. J Hum Evol 65:391-403.

Latimer B. 1991. Locomotor adaptations in *Australopithecus afarensis*: the issue of arboreality. In: Coppens, Y., Senut, B. (Eds.), Origine(s) de la Bipe´die chez les Hominide´s. CNRS, Paris, pp. 169-176.

Lazenby RA, Skinner MM, Kivell TL, Hublin J-J. 2011. Scaling VOI size in 3D μCT studies of trabecular bone: a test of the oversampling hypothesis. Am J Phys Anthropol 144:196-203.

Lieberman DE. 1996. How and why humans grow thin skulls: experimental evidence for systemic cortical robusticity. Am J Phys Anthropol 101:217–236.

Lovejoy CO, Meindl RS, Ohman JC, Heiple KG, White TD. 2002. The Maka femur and its bearing on the antiquity of human walking; applying contemporary concepts of morphogenesis to the human fossil record. Am J Phys Anthropol 119:97-133.

Liu XS, Bevill G, Keaveny TM, Sajda P, Guo XE. 2009. Micro- mechanical analyses of vertebral trabecular bone based on individual trabeculae segmentation of plates and rods. J Bio- mech 42:249–256.

Maga M, Kappelman J, Ryan TM, Ketcham RA. 2006. Preliminary observations on the calcaneal trabecular microarchitecture of extant large-bodied hominoids. Am J Phys Anthropol 129: 410–417.

McHenry HM. 1983. The capitate of *Australopithecus afarensis* and *A. africanus*. Am J Phys Anthropol 62:187-198.

McHenry HM. 1992. Body size and proportions in early hominids. Am J Phys Anthropol 87:407-431.

McHenry HM, Berger LR. 1998. Body proportions of *Australopithecus afarensis* and *A*. *africanus* and the origin of the genus *Homo*. J Hum Evol 35:1-22.

Michilsens F, D'Août K, Vereecke EE, Aerts P. 2012. One step beyond: Different step-to-step transitions exist during continuous contact brachiation in siamangs. Biol Open 1:411-421.

Mittermeier RA, Fleagle JG. 1976. The locomotor and postural repertoires of *Ateles geoffroyi* and *Colobus guereza*, and a reevaluation of the locomotor category semibrachiation. Am J Phys Anthropol 45:235-256.

Myatt JP, Crompton RH, Payne-Davis RC, Vereecke EE, Isler K, Savage R, D'Août K, Günther MM, Thorpe SKS. 2012. Functional adaptations in the forelimb muscles of non-human great apes. J Anat 220:13-28.

Niemitz C. 2010. The evolution of the upright posture and gait: a review and a new synthesis. Naturwissenschaften 97:241– 263.

Odgaard A. 1997. Three-dimensional methods for the quantification of cancellous bone architecture. Bone 20:315–328.

Odgaard A, Kabel J, van Rietbergen B, Dalstra M, Huiskes R. 1997. Fabric and elastic principal directions of cancellous bone are closely related. J Biomech 30:487–495.

Pahr DH, Zysset PK. 2009a. From high-resolution CT data to finite element models: development of an integrated modular framework. Comput Methods Biomech Biomed Engin 12:45-57.

Pahr DH, Zysset PK. 2009b. A comparison of enhanced continuum FE with microFE models of human vertebral bodies. J Biomech 42: 455-462.

Pontzer H, Lieberman DE, Momin E, Devlin MJ, Polk JD, Hallgrimsson B, Cooper D. 2006. Trabecular bone in the bird knee responds with high sensitivity to changes in load orientation. J Exp Biol 209:57–65.

Preuschoft H, Hohn B, Scherf H, Schmidt M, Krause C, Witzel U. 2010. Functional analysis of the primate shoulder. Int J Primatol, 31:301-320.

Räth C, Baum T, Monetti R, Sidorenko I, Wolf P, Eckstein F, Matsuura M, Lochmüller E-M, Zysset PK, Rummeny EJ, Link TM, Bauer JS. 2013. Scaling relations between trabecular bone volume fraction and microstructure at different skeletal sites. Bone 57:377–383.

Remis M. 1995. Effects of body size and social context on the arboreal activities of lowland gorillas in the Central African Republic. Am J Phys Anthropol 97:413-433.

Richard A. 1970. A comparative study of the activity patterns and behavior of *Alouatta villosa* and *Ateles geoffroye*. Folia Primat 12:241-263.

Ruff CB, Holt B, Trinkaus E. 2006. Who's afraid of the big bad Wolff?: "Wolff's law" and bone functional adaptation. Am J Phys Anthropol 129:484–98.

Ryan TM, Shaw CN. 2012. Unique suites of trabecular bone features characterize locomotor behavior in human and non-human anthropoid primates. PLoS ONE 7:e41037.

Ryan TM, Shaw CN. 2013. Trabecular bone microstructure scales allometrically in the primate humerus and femur. Proc R Soc Lond B Biol Sci 280: 20130172.

Ryan TM, Shaw CN. 2015. Gracility of the modern *Homo sapiens* skeleton is the result of decreased biomechanical loading. Proc Nat Acad Sci 112:372-377.

Ryan TM, Walker A. 2010. Trabecular bone structure in the humeral and femoral heads of anthropoid primates. Anat Rec 293:719-729.

Scherf H, Tilgner R. 2009. A new high-resolution computed to- mography (CT) segmentation method for trabecular bone architectural analysis. Am J Phys Anthropol 140:39–51.

Scherf H, Harvati K, Hublin J-J. 2013. A comparison of proximal humeral cancellous bone of great apes. J Hum Evol 65:29-38.

Scherf H, Wahl J, Hublin J-J, Harvati K. 2016. Patterns of activity adaptation in humeral trabecular bone in Neolithic humans and present-day people. Am J Phys Anthropol 159:106-115.

Skerry TM, Lanyon LE. 1995. Interruption of disuse by short duration walking exercise does not prevent bone loss in the sheep calcaneus. Bone 16:269–274.

Smith RJ, Jungers WL. 1997. Body mass in comparative primatology. J Hum Evol 32:523-559.

Soslowsky LJ, Flatow EL, Bigliani LU, Pawluk RJ, Ateshian GA, Mow VC. 1992. Quantitation of in situ contact areas at the glenohumeral joint: A biomechanical study. J Orthopaedic Res 10:524-534.

Stern J. 2000. Climbing to the top: a personal memoir of *Australopithecus afarensis*. Evol Anthropol 9:113-133.

Stern JT, Susman, RL, 1983. The locomotor anatomy of *Australopithecus afarensis*. Am J Phys Anthropol 60: 279-317.

Sugardjito J, van Hooff JARAM. 1986. Age-sex class differences in the positional behavior of the Sumatran orang-utan (Pongo pygmaeus abelii) in the Gunung Leuser National Park, Indonesia. Folia Primatol 47:14-25.

Susman RL, Stern JT, Jungers WL, 1984. Arboreality and bipedality in the Hada hominids. Folia Primatol 43:113-156.

Swartz SM, Bertram JEA, Biewener AA. 1989. Telemetered *in vivo* strain analysis of locomotor mechanics of brachiating gibbons. Nature 342:270-272.

Thorpe SKS, Crompton RH. 2006. Orangutan positional behavior and the nature of arboreal locomotion in Hominoidea. Int J Phys Anthropol 131:382-401.

Tsegai ZJ, Skinner MM, Pahr DH, Hublin J-J, Kivell TL. 2018. Systemic patterns of trabecular bone across the human and chimpanzee skeleton. J Anat 232:641-656.

Toussiant M, Macho GA, Tobias PV, Partridge TC, Hughes AR. 2003. The third partial skeleton of a late Pliocene hominin (Stw 431) from Sterkfontein, South Africa. S Afr J Sci 99:215-223.

Tuttle RH, Watts DP. 1985. The positional behavior and adapative complexes of *Pan gorilla*. In: Kondo S, editor. Primate morphophysiology, locomotor analyses and human bipedalism. Tokyo: Tokyo University Press. p 261-288.

Usherwood JR, Bertram JEA. 2003. Understanding brachiation: insight from a collisional perspective. J Exp Biol 206: 1631-1642.

van der Meulen MCH, Morgan TG, Yang X, Baldini TH, Myers ER, Wright TM, Bostrom MPG. 2006.

Cancellous bone adaptation in vivo loading in a rabbit model. Bone 38:871-877.

Wallace IJ, Winchester JM, Su A, Boyer DM, Konow N. 2017. Physical activity alters limb bone structure but not entheseal morphology. J Hum Evol 107: 14-18.

Ward CV. 2002. Interpreting the posture and locomotion of *Australopithecus afarensis*: where do we stand? Yrbk Phys Anthropol 35:185-215.

Ward CV. 2013. Postural and locomotor adaptations of *Australopithecus* species. In: Reed KE, Fleagle JG, Leakey RE, editors. The Palaeobiology of *Australopithecus*. Dordrecht: Springer. p 235–245.

Ward CV, Kimbel WH, Johanson DC. 2011. Complete fourth metatarsal and arches in the foot of *Australopithecus afarensis*. Science 331:750-753.

Westerhoff P, Graichen F, Bender A, Rohlmann A, Bergmann G. 2009a. An instrumented implant for *in vivo* measurement of contact forces and contact moments in the shoulder joint. Med Eng Phys 31:207–213.

Westerhoff P, Graichen F, Bender A, Halder A, Beier A, Rohlmann A, Bergmann G. 2009b. *In vivo* measurement of shoulder joint loads during activities of daily living. J Biomech 42:1840–1849.

Whitehouse WJ. 1974. The quantitative morphology of anisotropic trabecular bone. J Microsc 101:153-168.

Figure 1. Morphological filters applied during the whole-epiphysis analysis shown on a paracoronal midslice. Original segmented image (A); outer surface of the cortical bone (B), inner surface, defining the cortical-trabecular boundary (C); cortical thickness image (outer surface – inner surface) (D), trabecular only image (original segmented image - cortical thickness) (E), final masked image in which cortex, trabeculae and non-bone (air) are assigned separate greyscale values (F), 3D mesh of cortex (red) and trabecular bone (yellow) (H).

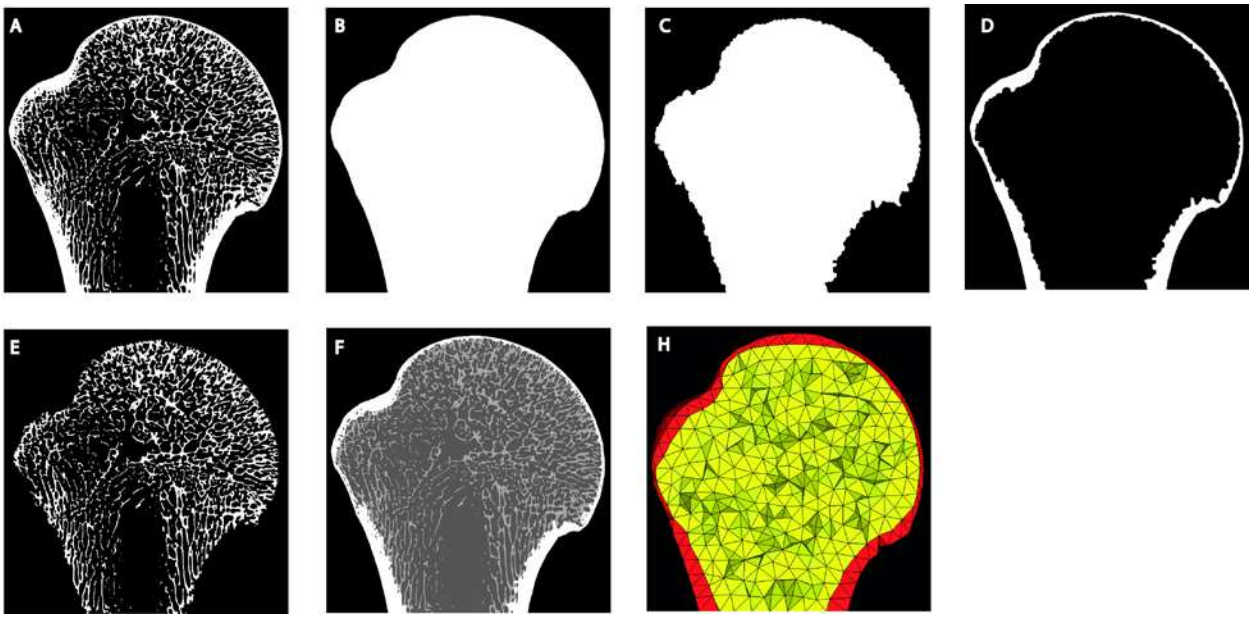

Figure 2. Example of the location of a cubic volume of interest. Subsequently, a spherical volume of interest (red circle) is extracted from this cube and having a diameter 30% of the geometric mean of the articular surface dimensions.

Figure 3. Coronal plane midslice though segmented image of one specimen of each extant taxon in the study sample and *A. africanus* StW 328. 1cm scale bar shown for each specimen.

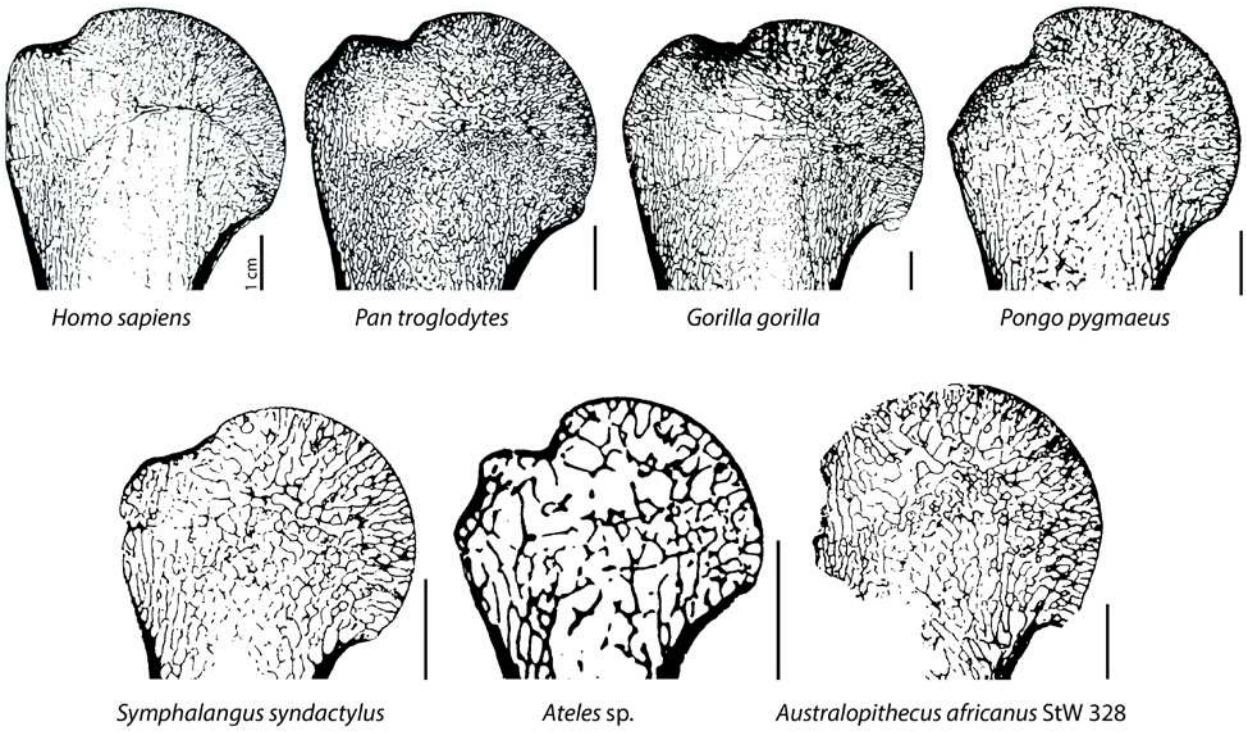

Figure 4. Box-and-whisker plots of trabecular variables across taxa and a comparison of bone volume fraction (BV/TV), trabecular thickness (Tb.Th), and anisotropy (DA) values dervied from the volume of interest and whole-epiphysis analyses. 'Tb.N;, trabecular number; 'Tb.Sp', trabecular separation; 'Tb.Pf', trabecular pattern factor; Symph.', *Symphalangus.*

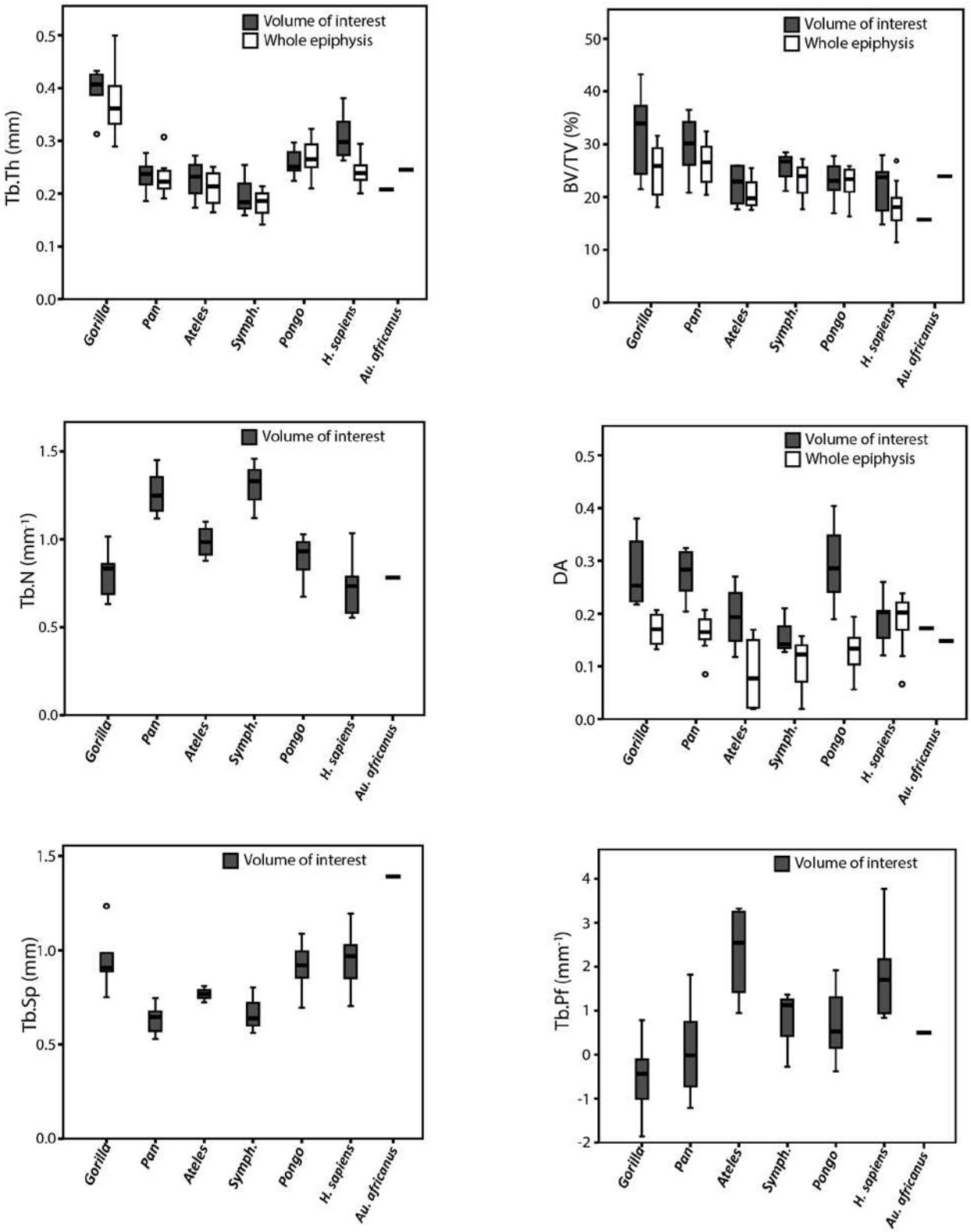
Volume of interest
Whole epiphysis
Tb.Th (mm)
BV/TV (%)
Tb.N (mm⁻¹)
DA
Tb.Sp (mm)
Tb.Pf (mm⁻¹)
Gorilla
Pan
Ateles
Symph.
Pongo
H. sapiens
Au. africanus

1

2

Figure 5. Bivariate plot of bone volume fraction plotted and degree of anisotropy (fabric DA) quantified in the whole-epiphysis. Convex hulls are drawn around specimens of each taxon. Symph.', *Symphalangus*

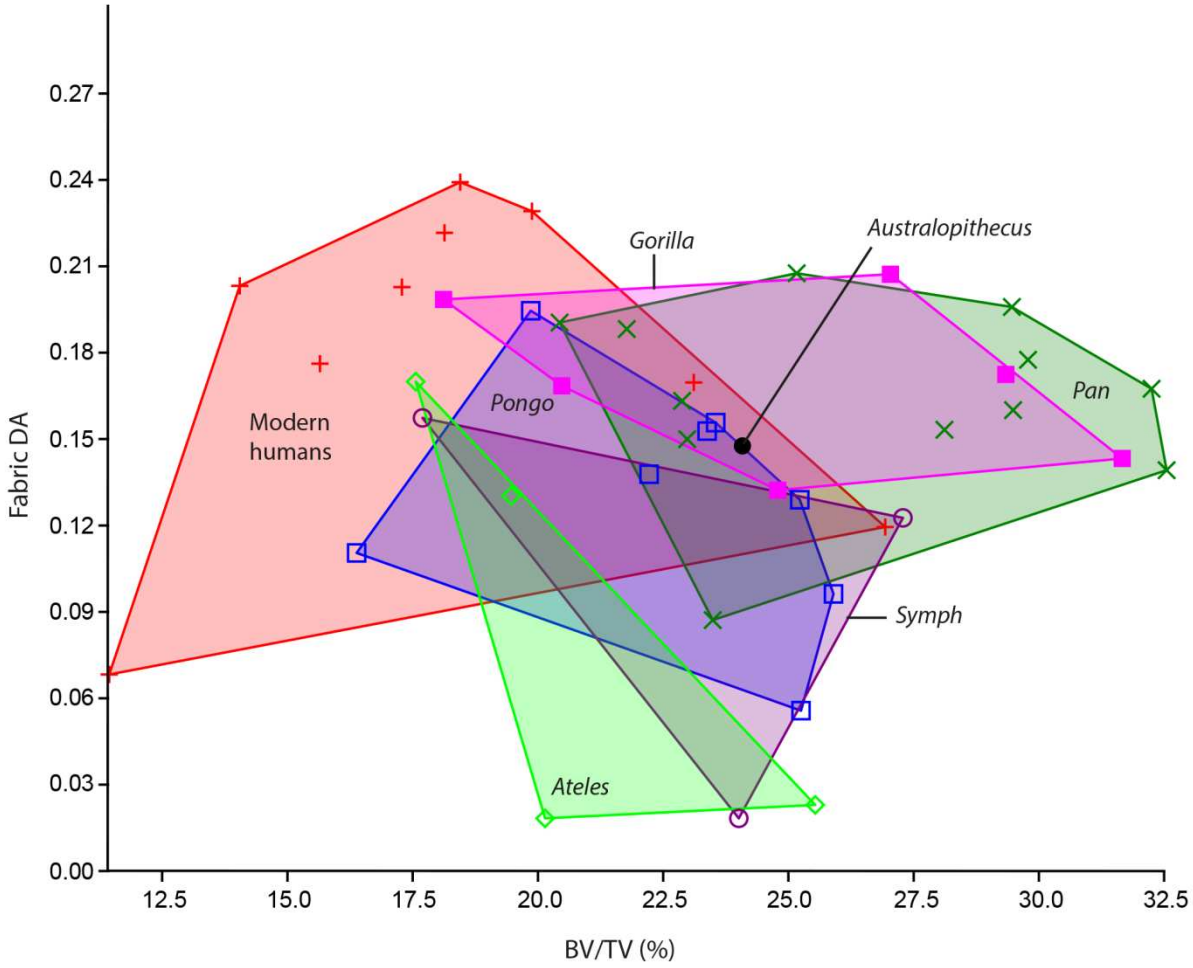

Figure 6. Visual representations of trabecular bone volume (BV/TV) in one specimen of each extant taxon in the study sample. From left to right: anterior view with main fabric and stiffness orientations, coronal plane cross-section, coronal plane midslice through segmented image, and superior view. In the first two colour maps (left), all specimens are scaled to a BV/TV range of 0-45%, while in the far-right colour maps (superior view), each specimen is scaled to its own data range to better show areas of BV/TV concentration. 'Pr', proximal; 'L;, lateral; 'M', medial; 'P', posterior; 'A', anterior.

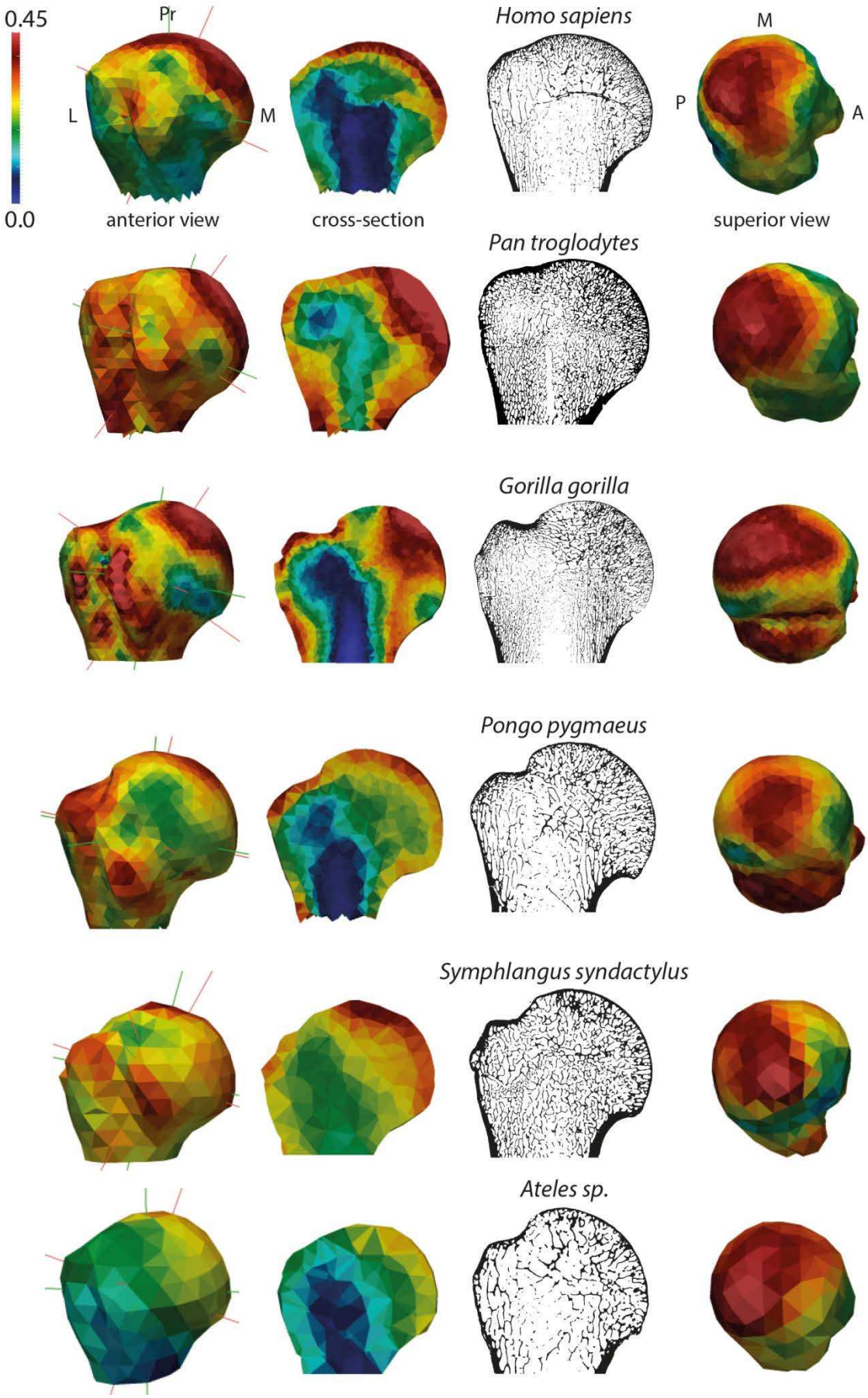
0.45
0.0
Pr
L
M
anterior view
cross-section
Homo sapiens
M
P
A
superior view
Pan troglodytes
Gorilla gorilla
Pongo pygmaeus
Symphlangus syndactylus
Ateles sp.

1

Figure 7. Detailed illustrations of the StW 328 specimen. Top row – surface models of StW 328 in, from left to right, anterior, medial, posterior and lateral views; middle row – midplane section illustrating preservation of trabecular structure (left) and superior view of surface model (right); bottom row – BV/TV maps in anterior view (far left), coronal cross-section (middle left), segmented coronal cross-section (middle), superior view (middle right), and parasagittal cross-section (far right).

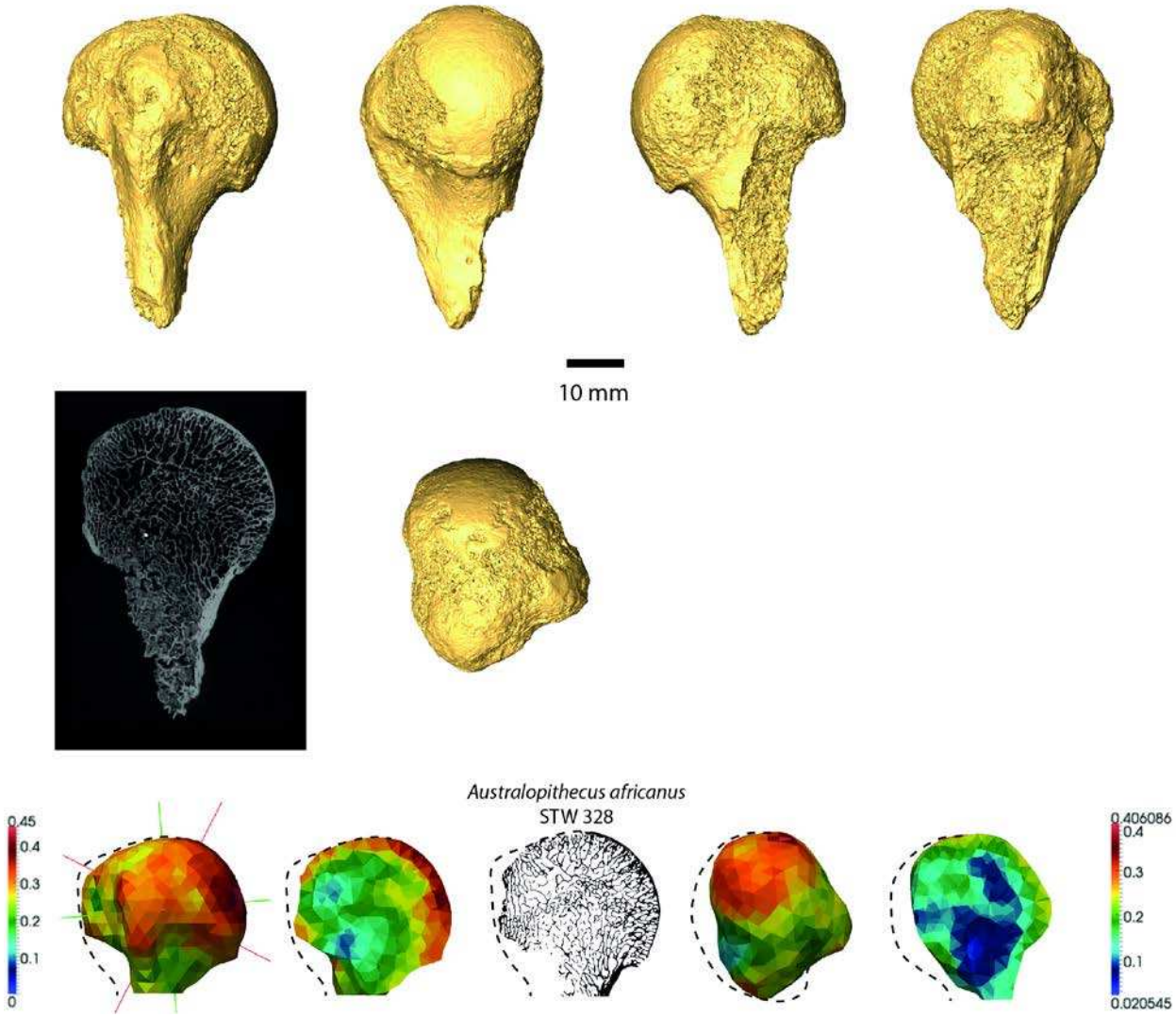

Figure 8. Principal component analysis scores of trabecular variables quantified in the volume of interest analysis. Convex hulls are drawn around all specimens of each taxon. 'Symph.', *Symphalangus.*

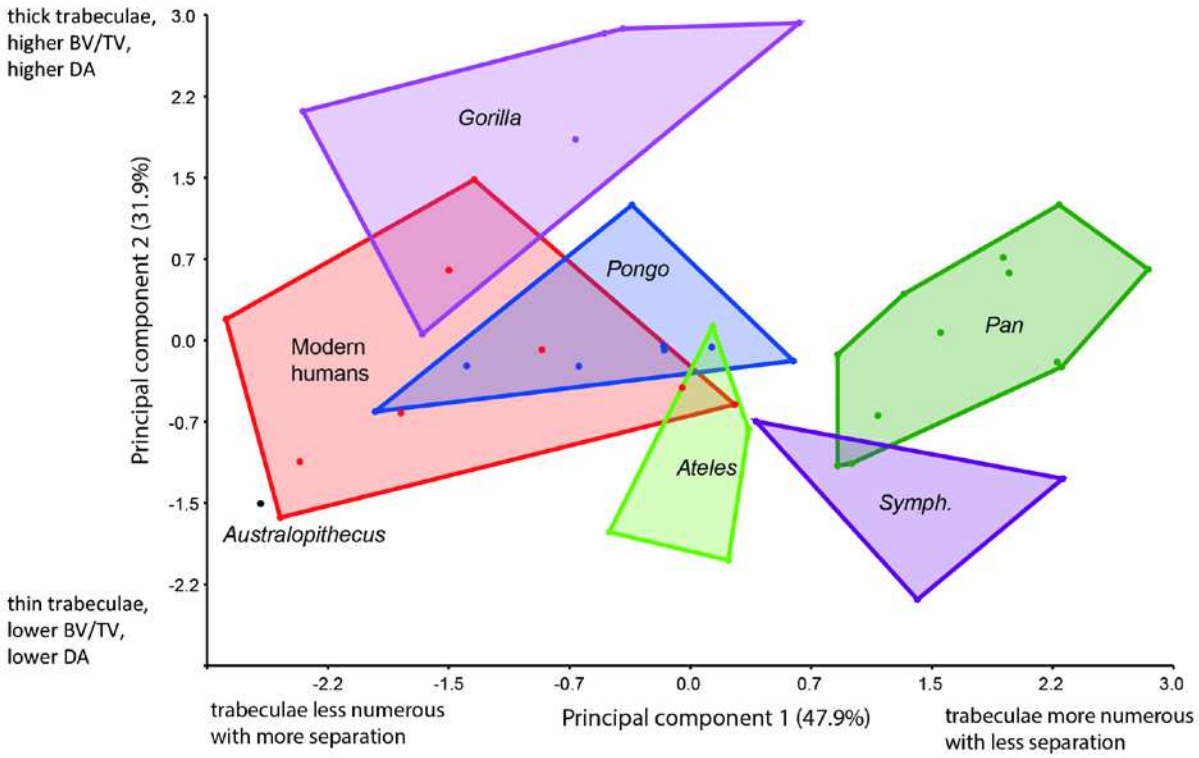

Table 1. Information about the study sample, including estimated body mass and primary locomotor mode.

Taxon	N	Side (R/L)	Sex (M/F/?)	Mean body mass (kg)[1] Male	Female	Locomotor mode
Homo sapiens	9	9/0	0/0/9	72.1[2]	62.1[2]	Bipedal
Australopithecus africanus	1	1/0	0/0/1	41[3]	30[3]	Bipedal/arboreal?
Pan troglodytes verus	12	5/7	0/0/12	46.3	41.6	Knuckle-walker
Gorilla gorilla	6	4/2	1/1/4	170.4	71.5	Knuckle-walker
Pongo pygmaeus	8	6/2	0/0/8	78.5	35.8	Suspensory (torso-orthogrady)
Symphalangus syndactylus	3	1/2	0/2/1	11.9	10.7	Suspensory (brachiation)
Ateles sp.	4	3/1	1/1/2	7.8-9.4[4]	7.3-9.3[4]	Suspensory (brachiation)[5]

[1]Extant primate body mass mean values from Smith and Jungers (1997)
[2]Data derived from contemporary Danes (Holloway, 1980)
[3]*Au.africanus* body mass estimates from McHenry (1992)
[4]Range covers all *Ateles* species reported in Smith and Jungers (1997)
[5]*Ateles* also uses a variety of other arboreal behaviours, including clambering and quadrupedal locomotion at similarly high frequencies to suspensory locomotion (Cant et al., 2001).

Table 2. Results of ordinary least squares regression for raw and logged trabecular variables derived from the whole-epiphysis (whole-epi.) and volume of interest (VOI) analyses.

Method	Variable	Isometric slope value[1]	Slope[2]	CL-	CL+	R^2	*y*-intercept	*P*	Result
whole-epi.	Raw Tb.Th	1	0.005	0.003	0.007	0.627	0.030	**<0.001**	-
	Log10 Tb.Th	1	0.809	0.525	1.020	0.642	-1.906	**<0.001**	-
VOI	Raw Tb.Th	1	0.006	0.004	0.007	0.68	0.03	**<0.001**	-
	Log10 Tb.Th	1	0.808	0.560	1.024	0.64	-1.87	**<0.001**	-
whole-epi.	Raw BV/TV	0	<0.001	-0.001	0.002	0.001	0.224	0.859	+
	Log10 BV/TV	0	0.024	0.271	0.329	0.001	-0.688	0.884	+
VOI	Raw BV/TV	0	0.001	-0.001	0.004	0.04	0.20	0.214	+
	Log10 BV/TV	0	0.136	-0.194	0.529	0.02	-0.82	0.445	+
whole-epi.	Raw Fab DA	0	0.001	0.001	0.003	0.037	0.114	0.226	+
	Log10 Fab DA	0	0.537	0.430	1.340	0.072	-1.710	0.089	+
VOI	Raw DA	0	0.002	<0.001	0.005	0.07	0.17	0.094	+
	Log10 DA	0	0.397	0.101	0.893	0.10	-1.26	0.043	+
VOI	Raw Tb.Pf	0	-0.029	-0.069	0.004	0.05	1.90	0.163	-
	Raw Tb.N	0	-0.016	-0.021	-0.008	0.32	1.63	**<0.001**	-
VOI	Log10 Tb.N	0	-0.673	-0.873	0.408	0.30	1.06	**<0.001**	-
	Raw Tb.Sp	1	0.011	0.005	0.016	0.28	0.37	**<0.001**	-
VOI	Log10Tb.Sp	1	0.569	0.266	0.775	0.30	-1.01	**<0.001**	-

[1]Following Ryan and Shaw (2013), for size variables (Tb.Th, Tb.Sp), isometric scaling slope = 1, + allometry = >1, - allometry = <1. For shape variables (BV/TV, DA, Tb.Pf, Tb.N), isometric scaling slope = 0, + allometry = >0, - allometry = <0.
[2]Slope indicates scaling coefficient for each variable with 95% confidence limits (CL-/CL+).

Table 3. Summary statistics for trabecular bone structure variables derived from whole-epiphysis (whole-epi.) and volume of interest (VOI) analyses.

		H. sapiens	*A. africanus*	*Pan*	*Gorilla*	*Pongo*	*Symphalangus*	*Ateles*
	Tb.Th (mm)							
whole-epi.	Mean	0.241 ± 0.029	0.248	0.229 ± 0.031	0.374 ± 0.073	0.269 ± 0.035	0.181 ± 0.037	0.211 ± 0.037
	Range	0.201 - 0.294	-	0.191 - 0.307	0.290 – 0.498	0.211 - 0.323	0.142 - 0.217	0.165 – 0.251
VOI	Mean	0.306 ± 0.044	0.213	0.235 ± 0.027	0.396 ± 0.045	0.258 ± 0.025	0.199 ± 0.050	0.227 ± 0.042
	Range	0.263 - 0.381	-	0.186 – 0.277	0.313 - 0.433	0.224 - 0.297	0.159 - 0.254	0.173 - 0.272
	BV/TV							
whole-epi.	Mean	0.183 ± 0.047	0.241	0.265 ± 0.042	0.252 ± 0.053	0.227 ± 0.032	0.230 ± 0.034	0.207 ± 0.034
	Range	0.114 - 0.269	-	0.204 - 0.325	0.181 – 0.316	0.163 - 0.260	0.177 - 0.273	0.176 – 0.255
VOI	Mean	0.220 ± 0.048	0.166	0.298 ± 0.052	0.324 ± 0.082	0.231 ± 0.035	0.254 ± 0.039	0.223 ± 0.043
	Range	0.148 - 0.279	-	0.208 – 0.365	0.215 - 0.433	0.169 - 0.278	0.211 - 0.284	0.176 - 0.259
	Fab DA							
whole-epi.	Mean	0.181 ± 0.056	0.148	0.165 ± 0.032	0.170 ± 0.029	0.129 ± 0.042	0.099 ± 0.072	0.085 ± 0.077
	Range	0.068 - 0.239	-	0.087 - 0.208	0.132 – 0.207	0.056 - 0.195	0.018 - 0.157	0.018 – 0.170
	DA							
VOI	Mean	0.191 ± 0.044	0.188	0.276 ± 0.040	0.277 ± 0.068	0.293 ± 0.074	0.160 ± 0.044	0.189 ± 0.063
	Range	0.121 - 0.260	-	0.204 – 0.324	0.215 - 0.372	0.189- 0.404	0.127 - 0.210	0.118 - 0.270
VOI	**Tb.Pf (mm^{-1})**							
	Mean	1.965 ± 1.113	0.554	-0.039 ± 0.951	-0.512 ± 0.892	0.687 ± 0.763	0.742 ± 0.888	2.336 ± 1.124
	Range	0.835 - 3.772	-	-1.210 – 1.820	-1.860 - 0.786	-0.385 - 1.916	-0.273 - 1.371	0.943 - 3.322
VOI	**Tb.N (mm^{-1})**							
	Mean	0.724 + 0.162	0.777	1.260 ± 0.111	0.810 ± 0.137	0.898 ± 0.121	1.302 ± 0.171	0.985 ± 0.096
	Range	0.552 - 1.033	-	1.117 – 1.449	0.630 - 1.015	0.673 - 1.027	1.119 - 1.456	0.876 - 1.099
VOI	**Tb.Sp (mm)**							
	Mean	0.944 ± 0.164	1.401	0.634 ± 0.070	0.945 ± 0.162	0.915 ± 0.121	0.667 ± 0.124	0.767 ± 0.036
	Range	0.704 - 1.194	-	0.529 – 0.745	0.750 - 1.234	0.695 - 1.088	0.561 - 0.802	0.723 - 0.809

Table 4. Pairwise comparisons across taxa of results from the whole-epiphysis and volume of interest (VOI) methods for trabecular thickness (Tb.Th), bone volume fraction (BV/TV), and degree of anisotropy (DA). In each table, the upper half presents comparisons across taxa in the VOI analysis and the lower half presents comparisons across taxa for the whole-epiphysis analysis.

Tb. Th	*H. sapiens*	*Pan*	*Gorilla*	*Pongo*	*Symphalangus*	*Ateles*
H. sapiens		-17.4**	NS	NS	-23.8**	-19.8*
Pan	NS		26.67**	NS	NS	NS
Gorilla	19.3**	24.8**		20.3**	33.0**	29.0**
Pongo	NS	-13.1*	NS		NS	NS
Symphalangus	NS	NS	36.3**	-24.7**		NS
Ateles	NS	NS	27.7**	-16.0*	NS	

BV/TV	*H. sapiens*	*Pan*	*Gorilla*	*Pongo*	*Symphalangus*	*Ateles*
H. sapiens		16.3**	17.9*	NS	NS	NS
Pan	20.5**		NS	13.9*	NS	15.7*
Gorilla	17.2*	NS		15.6*	NS	17.3*
Pongo	NS	NS	NS		NS	NS
Symphalangus	NS	NS	NS	NS		NS
Ateles	NS	15.0*	NS	NS	NS	

DA	*H. sapiens*	*Pan*	*Gorilla*	*Pongo*	*Symphalangus*	*Ateles*
H. sapiens		18.0**	16.9	19.3**	NS	NS
Pan	NS		NS	NS	22.1**	17.0*
Gorilla	NS	NS		NS	21.1*	NS
Pongo	-16.1*	NS	NS		-23.5**	-18.3*
Symphalangus	-20.0*	NS	NS	NS		NS
Ateles	-20.1*	15.0*	16.6*	NS	NS	

Note: light shading indicates a lack of agreement in statistically significant differences between the VOI and whole-epiphysis analysis; ‘NS’, not significant; ‘*’, indicates significant difference between taxa at $p < 0.05$; ‘**’, indicates significant difference between taxa at $p < 0.01$.

Table 5. Variable loadings on first two principal components listed by magnitude (VOI analysis).

Variable	PC1 (55.3%)	Variable	PC2 (27.2%)
TbN	-0.63	DA	0.92
Tb.Sp	0.61	TbTh	0.37
TbTh	0.47	TbN	0.14
DA	-0.04	Tb.Sp	-0.08